AGU
ADVANCING EARTH AND SPACE SCIENCE

Earth's Future

Key Points:

- Past mass extinctions are correlated with atmospheric CO_2 concentration, but not with long-term temperature nor with radiative forcing by CO_2
- Present CO_2 concentration is associated in the fossil record with a 6.39% genus loss, implying current human destruction of biodiversity
- Future anthropogenic mass extinction can be stopped only by cutting human emissions of CO_2 to zero, optimally by 2% per year starting now

Supporting Information:

Supporting Information may be found in the online version of this article.

Correspondence to:

W. J. Davis,
JacksonDavis@
EnvironmentalStudiesInstitute.org

Mass Extinctions and Their Relationship With Atmospheric Carbon Dioxide Concentration: Implications for Earth's Future

W. Jackson Davis[1,2] (iD)

[1]Division of Physical and Biological Sciences, University of California, Santa Cruz, CA, USA, [2]Environmental Studies Institute, Santa Cruz, CA, USA

Abstract Industrialization has raised the concentration of carbon dioxide (CO_2) in Earth's atmosphere by half since 1770, posing a risk from ocean acidification to global biodiversity, including phytoplankton that synthesize approximately ($\sim$) 50% of planetary oxygen. This risk is estimated here from the fossil record and implications for our energy and economic future are explored. Over the last 534 million years (Myr), 50 extinction events present as peaks of genus loss-and-recovery cycles, each spanning $\sim$3–40 Myr. Atmospheric CO_2 concentration oscillates with percent genus loss, leading in phase by $\sim$4 Myr and sharing harmonic periodicities at $\sim$10, 26 and 63 Myr. Over the last 210 Myr, where data resolution is highest, biodiversity loss is correlated with atmospheric CO_2 concentration, but not with long-term global temperature nor with marginal radiative forcing of temperature by atmospheric CO_2. The end-Cretaceous extinction of the dinosaurs is anomalous, occurring during a 20-million year depression in atmospheric CO_2 concentration and rising global temperature. Today's atmospheric CO_2 concentration, $\sim$421 parts per million by volume (ppmv), corresponds in the most recent marine fossil record to a biodiversity loss of 6.39%, implying that contemporary anthropogenic CO_2 emissions are killing ocean life now. The United Nations Intergovernmental Panel on Climate Change projects that unabated fossil fuel use could elevate atmospheric CO_2 concentration to 800 ppmv by 2100, approaching the 870 ppmv mean concentration of the last 19 natural extinction events. Reversing this first global anthropogenic mass extinction requires reducing net anthropogenic CO_2 emissions to zero, optimally by 2% per year starting immediately.

Plain Language Summary The rising concentration of carbon dioxide (CO_2) in Earth's atmosphere from burning fossil fuels poses a risk to biodiversity from ocean acidification, threatening marine algae that produce $\sim$50% of planetary oxygen. This risk is estimated here based on the relationship between marine biodiversity loss and atmospheric CO_2 concentration in the fossil record. Biodiversity loss varies cyclically with atmospheric CO_2 concentration on million-year timescales, but is not correlated with long-term global temperature nor with radiative forcing (RF) of temperature by CO_2. Atmospheric CO_2 is therefore a plausible cause of past mass extinctions, while long-term temperature change and RF by CO_2 are excluded. Biodiversity and atmospheric CO_2 cycle at periods similar to each other and to geological and astrophysical cycles, consistent with causal linkages. The concentration of CO_2 in today's atmosphere corresponds to a decline in fossil biodiversity of 6.39%, implying that current human-induced emissions of CO_2 are killing ocean life now. The United Nations Intergovernmental Panel on Climate Change projects that continuation of the global fossil fuel economy could raise atmospheric CO_2 to concentrations approaching the average of past mass extinctions by the year 2100. Arresting this first human-induced global mass extinction requires eliminating net human-induced emissions of CO_2 starting immediately.

1. Introduction

The concentration of carbon dioxide (CO_2) in the Earth's atmosphere has risen by more than half since 1770, due mainly to increased combustion of fossil fuels and more intrusive land-use practices (IPCC, 1990a, 1990b, 1992, 2001, 2007, 2013, 2021, 2022). As a consequence, atmospheric CO_2 concentration has reached 421 parts per million by volume (ppmv) (NOAA, 2020, 2021), the highest level of the last approximately ($\sim$) 20 million years (Myr) (Figure 5 in W. J. Davis, 2017). Research and policy attention has focused on the hypothesized effects of anthropogenic CO_2 emissions on global climate (ibid., but see W. J. Davis, 2017; W. J. Davis et al., 2018, 2019; W. J. Davis & Davis, 2020). The "other CO_2 problem" (Doney et al., 2009; Zeebe & Zachos, 2013), acidification of

Software: W. Jackson Davis
Supervision: W. Jackson Davis
Validation: W. Jackson Davis
Visualization: W. Jackson Davis
Writing – original draft: W. Jackson Davis
Writing – review & editing: W. Jackson Davis

ocean water by atmospheric CO_2 (e.g., Brewer, 2013; Galgani et al., 2014; Gattuso et al., 2014; Jiang et al., 2019) and consequent harm to global biodiversity (e.g., Gattuso et al., 2014; Weinbauer et al., 2012), has received comparatively less attention (Scherer et al., 2022).

Atmospheric CO_2 dissolves at the air-water interface of the ocean to produce carbonic acid, increasing the hydrogen ion concentration (acidity), or lowering the pH, of surface waters. The acidified water degrades the ecology of the critical upper few millimeters of the water column, the sea-surface microlayer (SSM) (Galgani et al., 2014; Rae et al., 2021; Rahlff et al., 2019; Smyrnova et al., 2017), where 90% of marine organisms spend a portion of their life cycle as vulnerable gametes, embryos, or juveniles (Weinbauer et al., 2012; Wurl et al., 2017). The adverse impact of atmospheric CO_2 on organisms in the SSM is thereby amplified throughout diverse global marine ecosystems. Acidified surface waters then mix in the global ocean on decadal, centennial and millennial time scales, damaging coral reefs (Vernon, 2008; Wolfram et al., 2022), coralline algae (Peña et al., 2021), deep sea ecology (Harvey et al., 2021), global biodiversity (Zunino et al., 2021), and reliant human populations (Doney et al., 2020).

The potential effects of ocean acidification on phytoplankton communities (Dutkiewicz et al., 2015; Figuerola et al., 2021; Flynn et al., 2012; Harvey et al., 2021; Shi et al., 2010) merit special attention. These keystone species form the base of the marine trophic system or food web (e.g., Kroeck et al., 2022), are responsible for ∼90% of primary production in the ocean (Duarte & Cebrian, 1996), and generate at least half of atmospheric oxygen (Baumert & Petzoldt, 2008; Falkowski et al., 1998; Field et al., 1998). The effects of ocean acidification on living plankton populations have proven hard to study directly. Long-term in situ mesocosm experiments yield inconsistent phytoplankton responses to ocean acidification and competing CO_2 fertilization (e.g., Alvarez-Fernandez et al., 2018; Eberlein et al., 2017). The mixed results have several possible explanations (Donahue et al., 2019; Hattich et al., 2017; Mélancon et al., 2016; Schlüter et al., 2016), but have nevertheless prompted investigators to question whether experimental findings from small, genetically homogeneous phytoplankton assemblages can be extended to the population level (Hattich et al., 2017).

An alternative approach to understanding the risks of atmospheric CO_2 to phytoplankton and the biodiversity they support relies on the fossil record. Growing evidence suggests that increased atmospheric CO_2 concentration and consequent ocean acidification was associated repeatedly throughout paleohistory with the collapse of plankton populations and the loss of global biodiversity (Brenchley et al., 2001; Kiessling & Simpson, 2011; Kroeck et al., 2022; Prokoph et al., 2004; Tapan, 1968). Elevated atmospheric CO_2 followed by acidification and consequent anoxia is a proposed kill mechanism of the three most recent and best-known of the canonical five mass extinctions, the Permian-Triassic (P-T) (Bond & Wignall, 2010), the Triassic-Jurassic (T-J) (Fox et al., 2022; Kaiho et al., 2021) and the Cretaceous-Paleogene (K-Pg) (Henehan et al., 2019). Consensus is growing that elevated CO_2 concentration is the immediate kill mechanism of most and perhaps all mass extinctions (e.g., Bond & Grasby, 2017a, 2017b; Fox et al., 2022). Marine extinctions are linked closely with terrestrial ones, explained by rapid two-way teleconnection of the underlying causes (e.g., CO_2, anoxia, sulfur dioxide) through the atmosphere (Algeo et al., 2011; Beauchamp & Grasby, 2012; Benton & Newell, 2014; Dal Corso et al., 2022). Modeling studies suggest that volcanic venting of CO_2 to the atmosphere coincident with the P-T mass extinction occurred on the same scale as contemporary anthropogenic CO_2 emissions (Capriolo et al., 2022). The seminal question for current energy and economic policy is whether acidification of ocean water from anthropogenic emissions of CO_2 now poses a comparable risk to contemporary global biodiversity, including humans.

This question is addressed here using large fossil proxy datasets that have been assembled in the last decade documenting the concentration of CO_2 in the Earth's atmosphere for the past 425 Myr (Royer, 2014) and global temperature over the Phanerozoic Eon, the last 540 Myr (Prokoph et al., 2008; Veizer et al., 1999). These advances enable quantitative comparisons between atmospheric CO_2 concentration, global temperature, and genus extinction over the last 534 Myr, supporting strong inferences about the possible contemporary threat. This approach is based on the rationale that the underlying biological, ecological and physical processes and natural laws have not changed appreciably on the Myr timescales evaluated here, and therefore the past effects of atmospheric CO_2 concentration on marine biodiversity as reflected in the marine fossil record provide a precise natural metric for estimating present and future effects. Using this rationale, proxy data from the past are used here to estimate the possible present risks to global biodiversity from anthropogenic CO_2 emissions, and to identify the most effective future carbon-reduction scenarios capable of mitigating this risk.

Evidence from the fossil record adduced using this approach suggests that the current, human-induced spike in atmospheric CO_2 concentration has already caused a significant loss of marine biodiversity approaching the

threshold for mass extinctions of the past, and that this loss of biodiversity is ongoing and growing rapidly. Human-induced CO_2 emissions are responsible for nearly all of the rise in atmospheric CO_2 concentration since the Industrial Revolution (IPCC, 2021, 2022), implying that the only way to arrest this first anthropogenic mass extinction of global biodiversity is to curtail net anthropogenic emissions of CO_2. The preliminary balancing here of potential socio-economic costs and biodiversity benefits of reducing anthropogenic CO_2 emissions suggests an optimum emission reduction rate of 2% annually, beginning immediately. Implementing this CO_2-reduction protocol would realize a carbon-neutral global economy by the year 2072 and limit human-induced loss of marine biodiversity to ~7.37%, a significant but nonetheless smaller loss than the ~8.3% mean genus loss shown here to characterize the smallest nine mass extinctions of the last 210 Myr.

2. Materials and Methods

2.1. Definitions and Terminology

A quantitative analysis of mass extinctions requires precise definition of terms. The most widely-accepted general definition of a mass extinction is J. J. Sepkoski's (1986):

> "A mass extinction is any substantial increase in the amount of extinction (i.e., lineage termination) suffered by more than one geographically wide-spread higher taxon during a relatively short interval of geologic time, resulting in an at least temporary decline in their standing diversity."
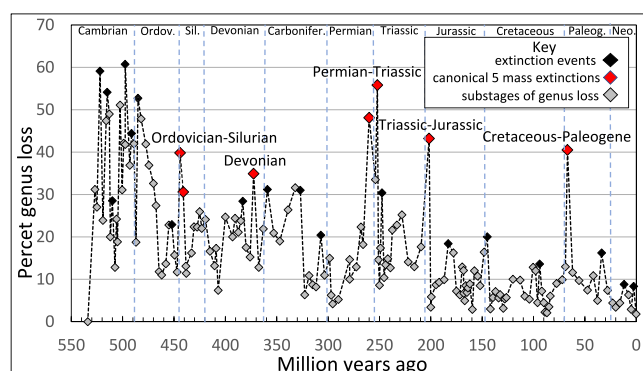
> (J. J. Sepkoski, 1986, p. 278)

Bambach (2006) observed that this general definition is vague in respect to measurable variables, and proposed that "an interval of mass extinction should display a peak of extinction intensity compared to the intensities in intervals immediately before and after." (Bambach, 2006, p. 128). This simpler formulation is consistent with J. J. Sepkoski's (1986) more general criteria and is valid for all periodic phenomena, including the fossil record of extinction. A mass extinction is accordingly defined for analytic purposes in this paper as "any peak in biodiversity loss that is flanked by lesser values." As will be shown below, applying this objective definition resolves significant past inconsistencies in the interpretation of mass extinction data.

Previous investigators established that the spectrum of extinction intensities across the Phanerozoic Eon (540-0 million years ago, or Mya) is a continuum (Bambach et al., 2004; Raup, 1991), making assignment of any quantitative threshold of biodiversity loss to qualify as a "mass" extinction "purely arbitrary" (Bambach, 2006, p. 128; see also Stanley, 2016). Accordingly, this paper uses the phrases and term "mass extinction," "extinction," and "extinction event" interchangeably and synonymously. The moniker "Big Five" used colloquially to describe Newell's (1952) original five large mass extinctions is substituted here with the alternative "canonical mass extinctions." This usage avoids the ambiguity introduced by the occurrence of at least a half-dozen larger mass extinctions during the earlier Cambrian and Ordovician Periods, and possibly larger extinction events of algae, bacteria and early multicellular organisms prior to the Phanerozoic Eon (Brocks et al., 2017).

2.2. Digitization of the Fossil Record

The standard modern data source for extinctions over geologic time was compiled by J. J. Sepkoski (1986, 2002) and lists 36,000 marine genera. This sample size (*n*) compares favorably with today's ~29,290 known and ~57,860 estimated living marine genera (Mora et al., 2011, their Figure S1, sum of Genus column), although this number is presumably smaller than the number of genera that disappeared over the last 534 Myr. Bambach (2006) reviewed the quality of the Sepkoski database for errors, gaps and uncertainties and concluded that "Problems of incompleteness of the geologic record probably do not seriously obscure detecting peaks of genus extinction." (Bambach, 2006, p. 148). That conclusion is supported here and by many other investigators who have found that periodicities in the extinction record (Fourier spectral power peaks) closely match independently-measured periodicities in geological, atmospheric and astrophysical cycles (the "Grand Cycles"; Boulila, 2019). Such congruencies would be highly improbable if the corresponding independent datasets were compromised significantly by data-quality issues or error variance. Data from the fossil record, including percent genus loss and the corresponding time before present, are therefore based on J. J. Sepkoski (2002).

The Sepkoski database of marine biodiversity loss was re-created for analysis here (Table S1 in Supporting Information S1) from Melott and Bambach (2014) by hand-digitizing a highly-magnified digital replica of their Figure

Figure 1. Time series of mass extinctions and their substages over the past 534 million years. Labels identify the five canonical mass extinctions. Original data are from Bambach (2006) and Melott and Bambach (2014) based on J. J. Sepkoski (1986, 2002). Cf. with Figure 1, p. 178 of Melott & Bambach, 2014. The lines connecting datapoints in this time series are for visual clarity only and do not reflect the existence of real data between designated datapoints. Abbreviations: Ordov., Ordovician; Sil., Silurian; Carbonifer., Carboniferous; Paleog., Paleogene; Neo., Neogene.

1 (p. 178). As a measure of the accuracy of the re-digitization, the Sepkoski extinction dataset was digitized twice independently and the re-measurement error computed for both percent genus loss and the corresponding time before present. Repeat-measurement error of percent genus loss across the dataset (sample size or $n = 163$ Myr time bins) was 0.069% (relative error, sign of the measurement differences included) and 0.094% (absolute error, signs of measurement differences excluded), respectively (see the Supporting Information S1). Relative and absolute re-measurement error for the time before present associated with datapoints of percent genus loss were 0.009% and 0.037%, respectively (Supporting Information S1). The larger absolute re-measurement error is probably a more valid measure of variance, but both relative and absolute error are less than a tenth of one percent, too small to affect the conclusions of this study. The mean of the two measurements was used here as the value of each datapoint (shaded columns of Table S1 in Supporting Information S1). As expected, the graphed time series of the fossil record re-digitized here from Melott and Bambach (2014, their Figure 1, p. 178) is visually indistinguishable from the corresponding re-digitized Figure 1 of the present paper. The digitization of the Sepkoski database is published in this paper as Table S1 in Supporting Information S1 to facilitate validation, replication and confirmation of the results reported here.

2.3. Proxies of Atmospheric Carbon Dioxide Concentration

Proxies of atmospheric carbon dioxide (CO_2) concentration over geologic time ($n = 831$) are from the expanded and updated database assembled by Royer (2014). Approximately 90% of CO_2 proxies are $\delta^{13}C$ (~61%) and stomatal indices and ratios (~29%). Analysis of error variance provides no evidence that atmospheric CO_2 proxy data degraded with age by, for example, diagenetic settling (W. J. Davis, 2017, Section 2). Error analysis including 2σ (standard deviation) confidence limits (96%) of CO_2 proxy data are likewise summarized previously (ibid.). These assessments show that uncertainties in CO_2 proxy data are relatively small (Figures 1 and 2 of W. J. Davis, 2017) and are unlikely to have significantly affected the analysis or conclusions of the present study.

Sampling frequency and therefore the resolution of CO_2 proxy data in the dataset used here is highest over the most recent 210 Myr of the fossil record, as documented previously (W. J. Davis, 2017, Section 2). The sampling frequency of CO_2 proxy data from 210 to 425 Mya, as far back in time as CO_2 measurements are available, ranges from fair to poor, with about half of the older Myr time bins lacking a proxy CO_2 datapoint, which must therefore be interpolated from the nearest available datapoints (W. J. Davis, 2017). Interpolation of missing datapoints introduces unknown uncertainty into any inferences that may be drawn. Therefore, in respect to atmospheric CO_2 concentration, the main conclusions of this paper are based upon the most highly-resolved (densely-sampled) segment of the CO_2 proxy record, the last 210 Myr. Averaging of CO_2 proxy data was done by computing mean CO_2 proxies in time bins of six Myr and advanced in time increments of 3 Myr (the 3–6 protocol, W. J. Davis, 2017).

2.4. Proxies of Global Temperature

Temperature proxies used here are stable isotopes of oxygen ($\delta^{18}O$) from Prokoph et al. (2008). The sample size of this database is $n = 6,680$. A more comprehensive temperature proxy database ($n = 58,532$) incorporating the proxy data used here was subsequently published (Veizer & Prokoph, 2015), but did not alter appreciably the shape of the temperature time series (for comparison, see Figure 3 in W. J. Davis, 2017) and was not accompanied by additional CO_2 proxy measurements. The calculations reported in the present paper were therefore not repeated using the expanded temperature proxy database.

All temperature proxy isotopic values of were multiplied by negative unity ($\delta^{18}O * (-1)$) to make proxy values taken from marine sedimentary deposits directly rather than inversely proportional to temperature proxies measured from land-based sources such as ice cores. As detailed previously (W. J. Davis, 2017), this arithmetic transform has no effect on the size or significance of computed correlation coefficients, and has no effect on the

conclusions of the present study. Following earlier precedents (W. J. Davis, 2017; Veizer et al., 1999), isotopic temperature proxy data are represented here graphically using a moving averaging method, the same 3–6 protocol as described above for CO_2 proxies (W. J. Davis, 2017).

2.5. Marginal Radiative Forcing by Atmospheric Carbon Dioxide

Radiative forcing (RF) at the top of the troposphere is a more direct and meaningful measure of the effect of CO_2 on temperature and climate than the concentration of CO_2 in the atmosphere, and is therefore used here in addition to CO_2 concentration to assess the possible effects, if any, of climate (temperature) change on biodiversity. Several atmospheric absorption/transmittance codes have been developed to compute RF from known concentrations of atmospheric trace gases. In the present study, RF from atmospheric CO_2 was computed using MODTRAN, inasmuch as this code is "the most used and accepted model for atmospheric transmission" (Driggers et al., 2012, p. 179). Additionally, MODTRAN is implemented online at the University of Chicago website (University of Chicago, 2022) in user-friendly format, facilitating replication and confirmation of the present results.

MODTRAN values for instantaneous RF were computed in Watts per square meter (W/m^2) at the top of the troposphere, as is conventional (IPCC, 2001, 2007, 2013). Three model locations (low, middle, high latitudes) and two model atmospheric conditions (cloudy and cloudless) were originally evaluated (W. J. Davis, 2017). Only one of these six options is used here, namely mid-latitude forcing under cloudless skies, because the corresponding RF there most closely approximates the global mean value (W. J. Davis, 2017). The RF at different concentrations of atmospheric CO_2 measured from the proxy record was computed using the MODTRAN model's default parameters, namely: CH_4 (parts per million) = 1.7, Tropical Ozone (parts per billion) = 28, Stratospheric Ozone scale = 1, Water Vapor Scale = 1, Freon Scale = 1, and Temperature Offset = 0°C.

Marginal forcing by CO_2 (ΔRF_{CO2}), defined as the increment in forcing associated with a given increment in atmospheric CO_2 concentration, was used here as the independent variable, in part because it best incorporates the exponentially-diminishing returns of forcing with increasing atmospheric CO_2 concentration. The value of ΔRF_{CO2} for incremental values of atmospheric CO_2 concentrations was computed by difference analysis of the CO_2 forcing curve in which each datapoint was subtracted from the previous one to determine incremental or marginal changes associated with each corresponding increment in the concentration of atmospheric CO_2 (see Figure 8b in W. J. Davis, 2017).

2.6. Statistical Methods and Software

Conventional and basic parametric statistical methods were used, including regression and correlation analysis, chi-square and Student-t tests to assess differences between means, expected and realized frequencies, and the statistical discernibility ("significance") of computed correlation coefficients. All hypotheses were tested at the standard maximum alpha level of 0.05, although more exact computed probabilities are usually reported here. Statistical tests were non-directional (two-sided) unless otherwise specified. Fourier-transformed spectral power periodograms for the global temperature and atmospheric CO_2 concentration datasets used here were published previously and computed with SAS JMP software, version 12.2.0 (W. J. Davis, 2017; W. J. Davis & Davis, 2020).

In addition to spectral power peaks, progressive (lagged) cross-correlation was used to detect and evaluate periodicity in time series. Spectral analysis supports inferences in the frequency domain, while progressive cross-correlation enables insights into the time domain, such as the phase relationships between cross-correlated cycles, that are unavailable from spectral analysis. Progressive cross-correlation entails iterative computation of the Pearson correlation coefficient (r) between two datasets, where one dataset is shifted one datapoint relative to the other between iterations. Plotting successive values of r against the number of datapoints shifted (termed the lag order) establishes nonrandom periodicity if and only if r alternates repeatedly with lag order and exceeds discernibility ($p < 0.05$) in successive cross-correlation cycles. Lag order, a dimensionless variable (no units), is converted to time in years by dividing the duration of the time series in years by the number of lag orders represented in the cross-correlogram. Computation of 95% confidence limits for cross-correlation coefficients was done as described previously (W. J. Davis & Davis, 2020) using directional t-tests.

3. Results

This section begins with an overview and analysis of the marine fossil record of mass extinctions. It then shows that the concentration of CO_2 in the atmosphere is correlated discernibly with percent genus loss and uses simple
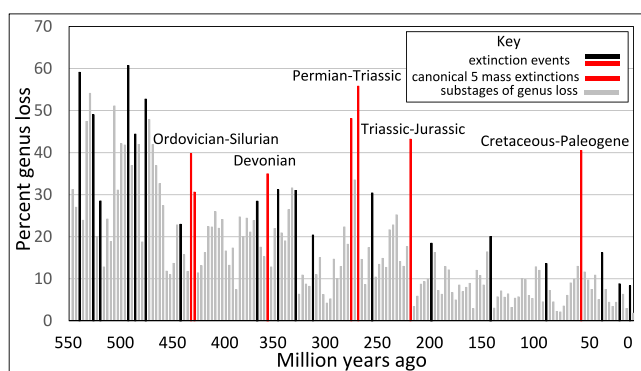
Figure 2. Equal-interval histogram of percent genus loss versus (vs.) time showing 25 previously-identified mass extinction events over the past 534 million years. The data plotted here are the same as in Figure 1. The original data (J. J. Sepkoski, 1986, 2002) were sampled at unequal time intervals that are obscured here by equally-spaced intervals on the abscissa, rendering the timescale in this histogram approximate (up to ±10%). Figure 1 shows the most accurate timescale. The five canonical mass extinctions are shown here by red bars and include two compound events (double bars on this Myr scale). Remaining mass extinctions that were identified previously (Bambach, 2006; Melott & Bambach, 2014; J. J. Sepkoski, 2002) are shown by black bars, while extinction "substages" are shown by gray bars. Cf. with Figure 1 of Bambach (2006, p. 135).

regression models to quantify the relationship. Evidence is then presented that biodiversity is not correlated with long-term global temperature nor with marginal RF of temperature by atmospheric CO_2. Section 3 concludes with application of the empirically-determined CO_2/biodiversity regression models to project and explore CO_2 emission reduction scenarios capable of arresting the inferred ongoing anthropogenic mass extinction.

3.1. The Fossil Record of Extinction Cycles

Nonrandom periodicity of extinction events over the last 534 Myr was suggested 70 years ago (Newell, 1952) and has been demonstrated repeatedly since (e.g., Melott & Bambach, 2014; Raup & Sepkoski, 1984). Spectral analysis of biodiversity time series shows discernible energy density peaks at ~10, 26 and 63 Myr (ibid.). Cycles corresponding to these peaks are visible in time series panels of the percent genus loss versus (vs.) time (Figure 1), although their periodicities or dominant frequencies can be established precisely only by spectral power analysis.

The most obvious feature of the fossil record time series is the reduced amplitude of extinction events over time, which has been noted by many previous investigators. This reduction in the magnitude of mass extinctions is accompanied by a gradual cooling of the globe by 8–9° over the past 534 Myr, and a decline over the same time period in atmospheric CO_2 concentration, from more than 2,000 ppmv (W. J. Davis, 2017) to as low as 180 ppmv during the depth of recent Great Ice Ages (GIAs) or Marine Isotope Stages (MISs of 80–120 thousand year [Kyr] periodicity). As a consequence of the declining amplitude of mass extinctions over geologic time, more recent mass extinction events are smaller in amplitude than more ancient peaks in biodiversity loss that have been identified previously not as extinction events but as "substages." This convention implies that older peaks in biodiversity loss that were not previously classified as mass extinctions are larger than more recent events that have been classified as mass extinctions, as is evident from Figure 1. This ambiguity is partially ameliorated by the operational definition of a mass extinction used here (Section 2) and has a straightforward potential physical explanation (see Section 4).

The time series of extinction events portrayed in Figure 1 depicts the canonical five mass extinctions (red symbols), 20 lesser extinction events (black symbols), and numerous "substages" that were not previously classified as mass extinctions by Melott and Bambach (2014) (gray symbols). Two of the recognized five canonical mass extinctions, the Ordovician-Silurian and Permian-Triassic, are compound events, that is, they consist of two adjacent or near-adjacent data points on Myr timescales that are conflated as a single large extinction event (Figure 1). The remaining three of the five canonical mass extinctions are unitary events on the Myr timescale of Figure 1. Lesser extinctions identified previously are all singular occurrences.

3.2. The Number and Frequency of Mass Extinction Cycles

An advantage of time series panels (Figure 1) is that the time of occurrence of extinction events is identified precisely despite variability in sampling frequency. The timescale is therefore valid for all datapoints. In contrast, interval histograms scaled using equally-spaced sampling intervals sacrifice timescale accuracy because variation in sampling intervals is obscured by the equal-interval labeling of the abscissa. Such interval histograms nonetheless render cyclic variation in percent genus loss more visible to the unaided eye (Figure 2). The most obvious periodic interval in such interval histograms is the ~26-Myr cycle reported previously (e.g., Melott & Bambach, 2014). The 25 extinction events shown in Figure 2 recur on a mean interval of 21.4 Myr (534 Myr record duration divided by 25 extinction events), comparable within likely error limits to the ~26-Myr periodicity identified by more precise spectral analyses.

Close examination of Figure 2 reveals a shorter periodicity that corresponds to the smaller ~10 Myr cycles detected by spectral analyses. When extinction cycles are defined operationally as a peak in percent genus loss flanked by lesser losses (Section 2), irrespective of the criteria of geographical breadth and amplitude of genus
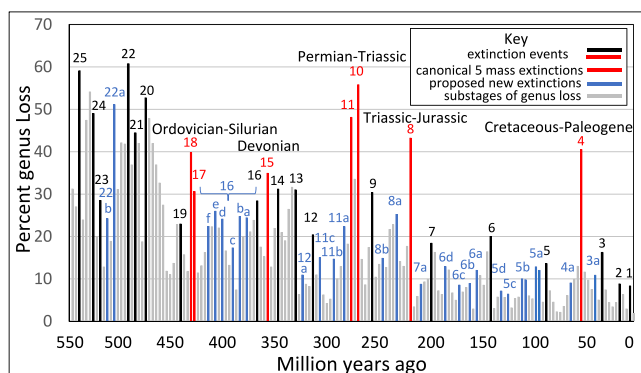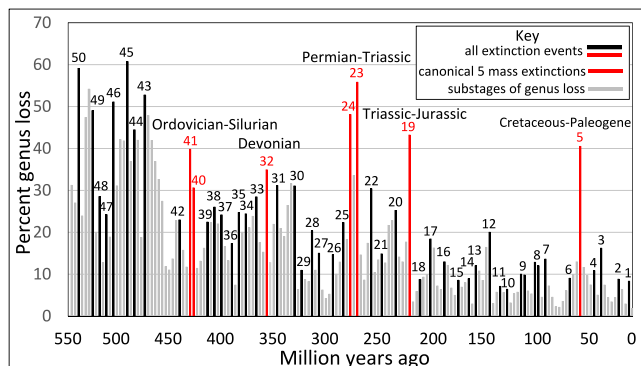
Figure 3. Interval histogram showing additional extinction events proposed in this study (blue bars). The newly-identified extinction events are local maxima in extinction cycles and are consistent in frequency with periodicities identified by matching spectral densities (see text). Otherwise as in Figure 2.

loss, the number of distinct extinction events doubles, to 50 over the last 534 Myr (blue bars in Figure 3). Calculating the mean repetition period of extinction events following this expansion yields an estimated periodicity of 10.6 Myr (534 Myr/50 extinction events), similar within likely error limits to the ~10 Myr periodicity identified by more accurate spectral power analysis. The definition of extinction events used here, a peak in biodiversity loss flanked by lesser values (see Section 2), therefore rationalizes periodicities reported previously from spectral analysis with periodicities visible to the unaided eye in time series such as Figure 3.

With the addition of these 25 newly-designated extinction events based on whether they comprise a local peak in the extinction time series, the present study identifies 50 mass extinction events over the last 534 Myr (Figure 4). Two of the newly-identified extinctions are compound (paired) events (# 8 and # 9 in Figure 4), in addition to two of the five canonical mass extinctions (Figure 4), while the remainder of all extinction events are unitary events on the Myr-timescale of Figure 4.

3.3. The Temporal Structure of Mass Extinction Cycles

At least some major mass extinctions of the past have been conceived as singular events caused by transient worldwide catastrophes. The Cretaceous-Paleogene (K-Pg) extinction of the dinosaurs, for example, is widely considered to have been caused by a collision of the Earth with an asteroid or comet (bolide; e.g., L. W. Alvarez et al., 1980), while the Permian-Triassic extinction is thought to have resulted from globally-synchronized volcanic eruptions (e.g., Fox et al., 2022). The demonstrated periodicity of extinctions shown previously and above, however, suggests that extinction is a continuous, repetitive process that manifests cyclically following dominant ~10 and particularly ~26 Myr periodicities. This suggests the hypothesis that each extinction cycle follows a similar pattern, namely, a long rise in biodiversity loss lasting ~5.34 Myr on average ([534 Myr/50 extinction events]/2) followed by an equally-lengthy ~5.34 Myr decline on average, assuming extinction cycle symmetry.

This hypothesis is confirmed by individual extinction events, which show a monotonic rise over millions of years to a peak of percent genus loss, defined as the extinction event, followed by a fall over Myr time periods to near-original baseline values (Figures 1–4). The percent genus loss during the K-Pg extinction ~66 Mya, for example, rose monotonically to a peak over a time period of 20 Myr and then declined monotonically to original levels of genus loss in the 19.5 Myr following the peak in biodiversity loss (e.g., Figure 4, time period from ~90 to 50 Mya). The duration of the K-Pg extinction cycle is therefore an unprecedented ~40 Myr. This finding from a single, prominent member of the canonical five mass extinctions suggests the hypothesis that mass extinctions in general are slow and incremental, rather than fast and singular. L. Alvarez et al. (1984) rationalized these two explanations of the K-Pg extinction with calculations showing that expected meteor showers are accelerated regularly for periods lasting up to 3 Myr.
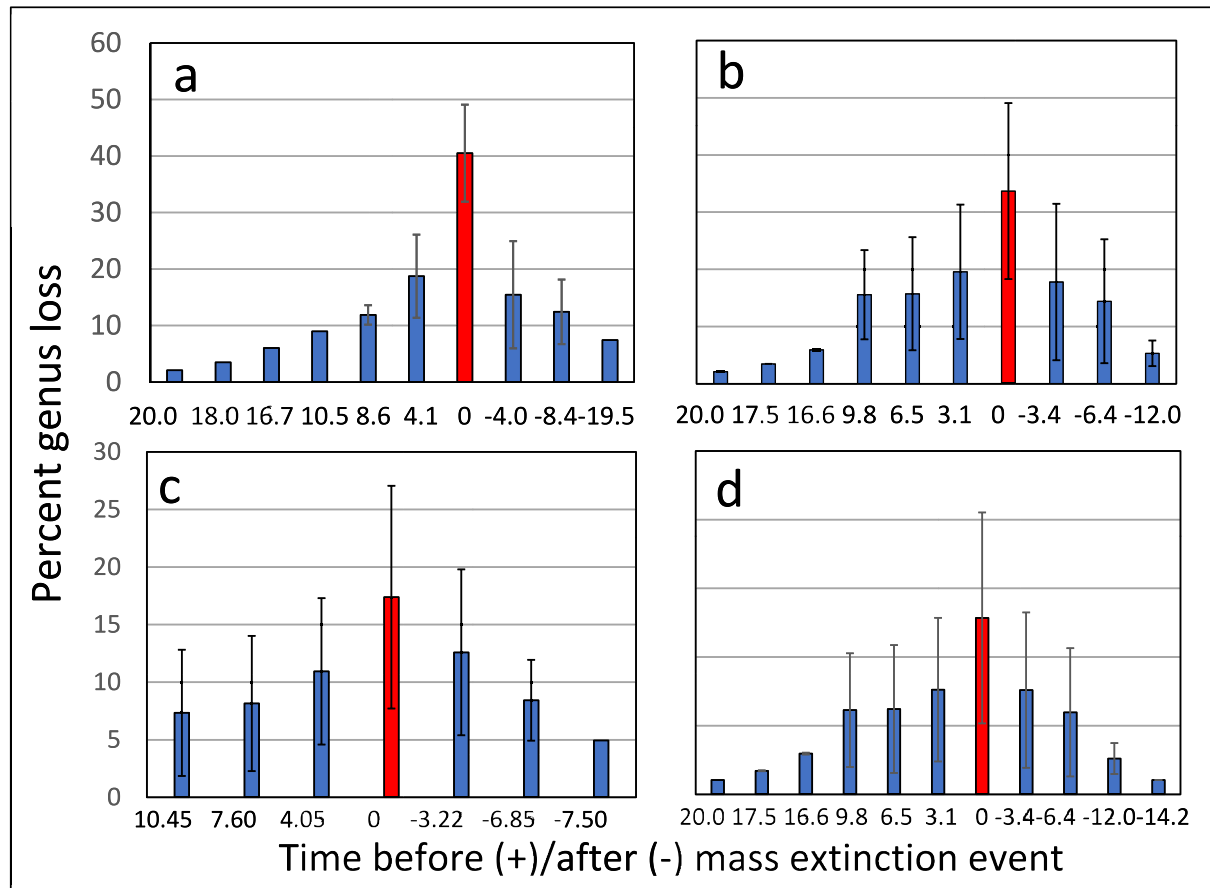
The hypothesis of gradual build-up and drawdown of past extinctions was tested by analyzing all mass extinctions recorded in the fossil record over the last 534 Myr (Figure 5), including the 25 newly-identified mass extinction events (Figure 4). The mean temporal form of all five of the canonical mass extinctions (Figure 5a) shows the same pattern as the K-Pg extinction, namely, a slow rise to a peak, defined as the extinction event, followed by a slow fall in percent genus loss to the original baseline. The difference between mean percent genus loss during the mass extinction event versus the means of every testable ($n > 1$) substage is discernible (directional heteroscedastic t-tests, $p < 0.05$; Table S2 in Supporting Information S1). Comparable analysis of the 25 mass extinction events identified previously (Melott & Bambach, 2014) shows the same rise of percent genus loss to a peak followed by a decline (Figure 5b), as for the K-Pg extinction (Figure 4) and collectively for the five canonical mass extinctions (Figure 5a). The difference between

Figure 4. Interval histogram showing all extinction events recognized in this study over the past 534 million years. Otherwise as in Figure 2.

Figure 5. Histograms showing the average temporal structure of four categories of mass extinctions (a–d). (a) The canonical five mass extinctions (Figures 1 and 2); (b) the previously identified 25 mass extinctions (Figures 1 and 2); (c) newly-identified mass extinction events from this study (Figure 3); (d) all 50 mass extinction cycles over the last 534 million years (Figure 4). Each graph shows the percentage genus loss during successive extinction substages (blue bars) and the mass extinction peak (red bar) over the indicated time period. Error bars equal 2σ (standard deviations). Positive and negative times on the abscissa of each graph designate time before and after the illustrated mass extinction event, respectively. The apparent visual asymmetry of the extinction cycles in a, b, and d is an artifact of the nonlinear timescale. The percent genus loss in substages is in all cases of n (sample size) greater than 1 is discernibly smaller ($p < 0.05$) than the mean loss at the peak of the extinction event. Computed probabilities are shown in Table S2 in Supporting Information S1. Absence of an error bar signifies that the corresponding $n = 1$.

mean percent genus loss during the mass extinction (red bar) versus the means of every testable substage (blue bars) is discernible ($p < 0.05$; Table S2 in Supporting Information S1).

Similar analysis of the 25 newly-identified mass extinction events proposed here (Figure 3) is shown in Figure 5c, while Figure 5d shows the comparable analysis of all 50 mass extinction events identified previously and in the present study (Figure 4). In all cases extinction cycles rise to a peak in genus loss over millions of years and decline back to a baseline over a slightly-shorter time period. In every case the mean loss at the peak of the extinction event is discernibly greater than the mean loss of previous and subsequent substages ($p < 0.05$) (Table S2 in Supporting Information S1). Therefore, all mass extinctions recorded in the marine fossil record of the past 534 Myr show the same pattern of a rise to a significantly larger peak (the extinction event) followed by a fall to near the original baseline. The apparent temporal asymmetry of the extinction cycle (Figures 5a, 5b, and 5d) is an artifact of the nonlinear time scale. In practice the rise time of all extinction cycles approximately equals the fall time, that is, mass extinction cycles are approximately symmetrical, with a slight but untested possible bias toward more rapid recovery (Figures 5b–5d).
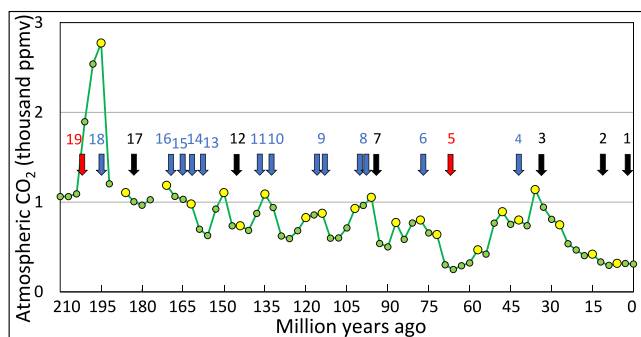
The above findings demonstrate that mass extinction events repeat systematically following a stereotypical cycle that builds to a peak and then declines over a similar time course of a million or more years. This rise/fall pattern applies to every mass extinction event recorded in the fossil record for the past 534 Myr and is therefore a universal feature of past mass extinction events. This pattern, identified previously for the K-Pg extinction (L. Alvarez
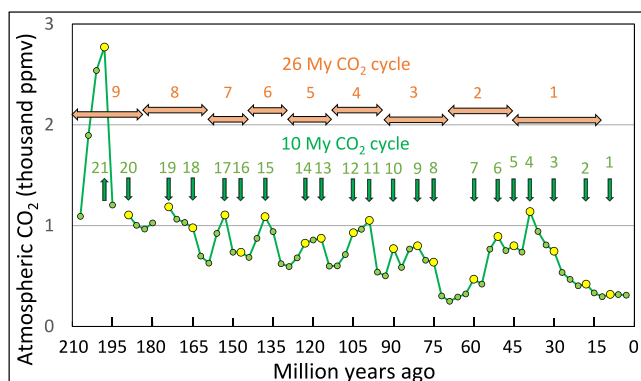
Figure 6. Time series showing the concentration of carbon dioxide (CO_2) in Earth's atmosphere for the past 210 million years. Green and orange arrows mark respectively the 10 and 26 Myr CO_2 cycle identified also in spectral periodograms (W. J. Davis, 2017). Peaks in the 10 Myr cycle are represented on the time series as yellow datapoints. The lines connecting datapoints in this time series are for visual clarity only and do not reflect the existence of real data between designated datapoints. Abbreviations: CO_2, carbon dioxide; Myr, million years.

et al., 1984) is confirmed here for all past mass extinctions, providing new constraints on the nature and causes of mass extinctions (Section 4).

3.4. Phase Relationship Between Extinction Cycles and Atmospheric Carbon Dioxide
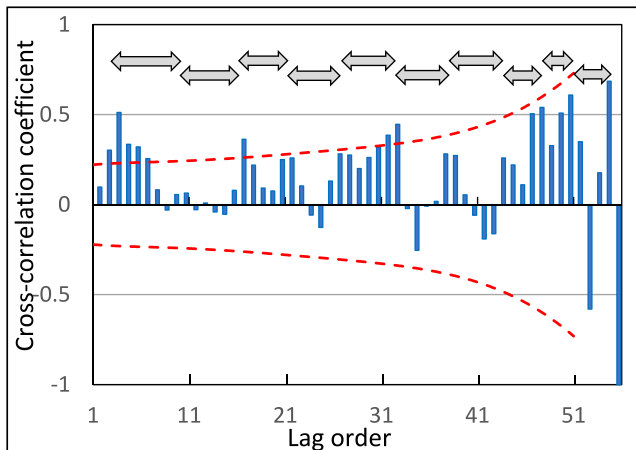
The above findings display graphically what has been established previously by spectral power analysis, namely, biodiversity loss varies cyclically over the 534-Myr fossil record. Three distinct periodicities are evident visually in time series and correspond approximately to the three spectral density peaks discovered previously by Fourier transform (Melott & Bambach, 2014), namely ~10, 26 and 63 Myr. It was reported earlier that the concentration of CO_2 in the ancient atmosphere varied cyclically with spectral density peaks at ~10–15, 26 and 63 Myr (W. J. Davis, 2017). This section addresses the phase relationships between these two coupled "Grand Cycles" (Boulila, 2019), the carbon cycle and the extinction cycle.

Time series of atmospheric CO_2 concentration (Figure 6) show the dominant ~26 Myr CO_2 cycle (horizontal double-headed arrows) and the smaller 10 Myr CO_2 cycle (vertical arrows).

Plotting the time of occurrence of mass extinctions on the same CO_2 time series (Figure 7) shows that over the last 210 Myr, where CO_2 data are best resolved, there were 19 extinction cycles, nine complete 26-Myr CO_2 cycles, and 21 10-Myr CO_2 peaks (Figures 6 and 7). Of the 19 extinction cycles, 13 (68.4%) coincide approximately with the 26-Myr CO_2 cycle, while six (# 1, 2, 5, 12, 13, 17) do not (Figure 7). Extinction peaks of 10 Myr periodicity cluster near the peaks of the 26-Myr CO_2 cycle (Figure 7), suggesting that the underlying mechanism(s) forcing the 10 Myr cycle is either the same or influenced by a common driving force. These findings demonstrate the association of CO_2 peaks with mass extinction events. They also show a delay of multi-Myr timescale between the four exceptional mass extinction events, including the K-Pg extinction of the dinosaurs, showing that these biodiversity losses were not accompanied by high levels of atmospheric CO_2 on Myr timescales, and instead have an additional or different explanation (see Section 4).

Progressive cross-correlation of atmospheric CO_2 concentration versus percent genus loss over the last 210 Myr shows discernible periodicity at approximately the 26-Myr period revealed by previous spectral analysis (Figure 8). The absence of a discernible cross correlation at a lag order of zero signifies that atmospheric CO_2 concentration and biodiversity loss do not oscillate in exact phase with each other. Discernible cross-correlation maximizes first at a lag order of 3 (Figure 8), implying that on average, the peak amplitude of biodiversity loss lags the peak in CO_2 concentration by ~3.21 Myr on the 26-Myr cycle (3 lag orders × 1.07 Myr per lag order). This estimated duration corresponds to a phase lag from atmospheric CO_2 concentration to peak biodiversity loss of 134.4° on average ([[3.21 Myr/26 Myr] × 360°]+90°). The addition of 90° is required to shift the zero reference point from the beginning of the sinusoid to the beginning of the cycle as shown in Figure 9.

This conclusion is confirmed and refined by the corresponding phase diagram of extinction cycles on the 26-Myr atmospheric CO_2 cycle. The peak of each extinction cycle over the last 210 Myr is superimposed on the 26-Myr CO_2 cycle represented schematically as a sinusoid (Figure 9). Of the 18 extinction cycles that occurred during complete 26-Myr CO_2 cycles across the most recent 210 Myr, 12 occurred on the rising phase of the 26 Myr CO_2 cycle (270–360° plus 0–90° of phase angle), while six occurred during the falling phase (90–270° of phase angle; Figure 9). Under a random distribution, equal numbers are expected in each group. The difference between observed and

Figure 7. Time series of the atmospheric concentration of carbon dioxide (CO_2) for the last 210 million years (Myr) with superimposed peaks of identified mass extinctions (arrows). Carbon dioxide (CO_2) proxy data are from Royer (2014), while extinction data are from Melott and Bambach (2014) after J. J. Sepkoski (1986, 2002). Extinction events are labeled by number from Figure 4 and coded by colored arrows. Key: red, two of the canonical five mass extinctions; black, previously-identified smaller extinction events; blue, extinction events newly-identified in this study. Two of the 19 extinction events (# 8 and 9) are compound, that is, they consist of two separate but adjacent extinction peaks on the Myr timescale used here. The lines connecting datapoints in this time series are for visual clarity only and do not reflect the existence of real data between designated datapoints. Abbreviations: CO_2, carbon dioxide; ppmv, parts per million by volume.

Figure 8. Progressive cross-correlogram of atmospheric carbon dioxide (CO_2) concentration versus (*vs.*) percent genus loss during the Cretaceous-Paleogene (K-Pg) mass extinction cycle. Cross-correlation was computed over the time period 90–30 million years ago. Lag order is equivalent to a time interval of 1.07 million years (Myr). The double-headed arrows designate visible sub-cycles in cross-correlation, which correspond approximately to the 10-Myr cycle of biodiversity loss. Red dashed lines show *95%* confidence limits for the discernibility of cross-correlation coefficients.

expected groups is statistically discernible with high probability ($X^2 = 18$, $p = 0.000022$), that is, mass extinctions are clustered near but somewhat after the peak of the CO_2 cycle.

Plotting these extinction peaks on the CO_2 cycle represented as a sinusoid (Figure 9b) illustrates that while most extinction events occur at or near the peak of the 26-Myr peak of the atmospheric CO_2 cycle, prominent exceptions include one of the five canonical mass extinctions, the K-Pg event (right red arrow in Figure 9b; see Section 4). The mean phase shift of all datapoints in Figure 9b is 146.45° (yellow arrow in Figure 9b), compared with 134.4° estimated above from the cross-correlogram. The more precise phase analysis (Figure 9) therefore shows that mass extinctions occur on average 4.08 Myr following peaks in atmospheric CO_2 concentration (56.45°/360° × 26 Myr).

3.5. Atmospheric CO_2 Concentration and Biodiversity Extinction

The above phase analysis shows that atmospheric CO_2 and extinction cycles oscillate together at the same frequencies, with percent genus loss lagging the CO_2 cycle in phase by ~4.08 Myr. The amplitude of these CO_2 peaks is positively correlated with the amplitude of the nearest peaks in percent genus loss ($r = 0.72$, $p = 0.0005$; Figure 10). Extinction events are evident first at a CO_2 concentration peak approaching 280 ppmv (Figure 10, far left datapoints), near the maximum CO_2 concentration during the warm interstadials between the GIAs (MISs). Therefore, fluctuations of CO_2 during natural climate cycles generally do not reach the threshold of significant biodiversity loss. The majority of extinction events occur in the CO_2 concentration range of 700–1,100 ppmv.

Two of the 19 extinction events recorded during the last 210 Myr were excluded from the scatterplot of Figure 10 because they are statistical outliers as defined by the 3-σ (standard deviation) convention, that is, their mean values exceed 3σ of the corresponding population mean (Ruan et al., 2005), and because each outlier datapoint exhibits additional statistical anomalies. One of the two omitted datapoints, event # 18 in Figure 4, is the smallest on record in terms of percent genus loss, yet one of the largest in the concentration of CO_2 in the atmosphere, 2,772 ppmv, five times the standard deviation of the population mean (554 ppmv). This weakest of all 50 extinction events is a unique artifact of the method used to define extinctions, that is, any peak in percent genus loss that is flanked by lesser percent genus losses, when the method is applied to small changes that are superimposed on rising (in this case) or falling extinction levels.

The second omitted outlier, the datapoint corresponding to the K-Pg extinction of the dinosaurs (# 5 in Figure 4), is excluded from the scatterplot of atmospheric CO_2 concentration versus percent genus loss (Figure 10) for three reasons. First, the atmospheric CO_2 concentration at the time of the K-Pg event, ~66 Mya in Figure 1, was the lowest of any extinction on record, 249 ppmv, yet the amplitude of the K-Pg extinction in terms of percent genus loss (40.5%) was second only to the T-J extinction (43.2%) over the last 210 Myr, making this datapoint a double outlier. Second, the K-Pg extinction event is unique in the duration and depth of carbon cycle perturbation (Figure 11). Depression of atmospheric CO_2 concentration starts at ~72 Mya, nearly 6 Myr prior to the age of the impact crater at Chicxulub, which is generally considered the cause of the extinction event. Recovery of the carbon cycle to pre-extinction levels required an additional ~12 Myr. Third, the correlation coefficient between peak atmospheric CO_2 concentration and peak percent genus loss across this time period is negative, $r = -0.55$ ($p < 0.05$; Figure 12), unlike any other time period evaluated here over the last 210 Myr (see below). Inclusion of these data would obscure or at least compromise any overall trend toward positive correlation.

The CO_2/extinction regression analysis was extended by associating every extinction datapoint over the last 210 Myr ($n = 66$) with the atmospheric CO_2 concentration datapoint nearest to it in time. The regression of CO_2 concentration on percent genus loss for specified time ranges was then computed. The average difference in timing between the coupled CO_2 and extinction datapoints over 210 Myr was 0.013% (relative difference, signs of percent differences included) and 2.57% (absolute difference, signs omitted). This analysis is therefore as close as possible with this dataset to the most powerful matched-pair correlation analysis. The advantage of this
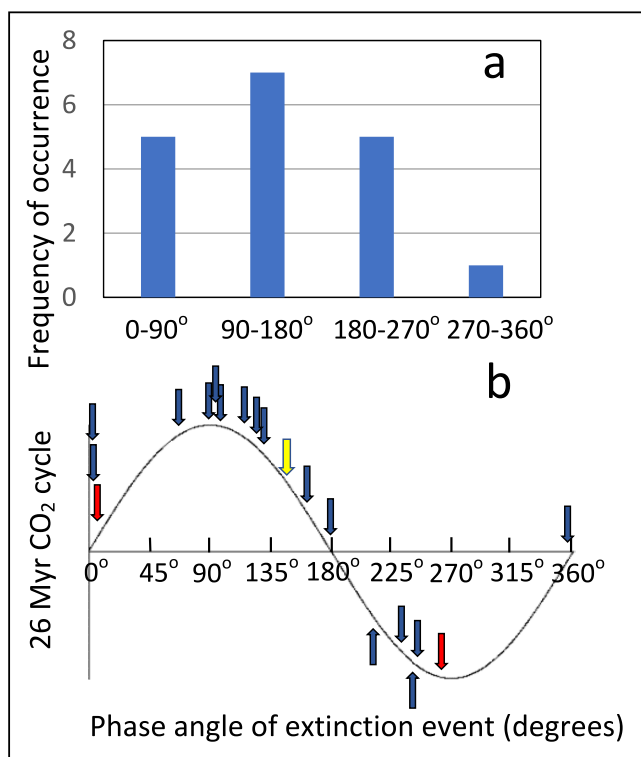
Figure 9. Quantitative relationship between the 26-Myr atmospheric CO_2 concentration cycle and mass extinction events. (a) Phase histogram. (b) Phase diagram of extinction events on the 26-Myr atmospheric carbon dioxide (CO_2) cycle (schematic sine wave). Red arrows correspond to two of the five canonical mass extinctions. The yellow arrow designates the mean phase angle of all extinction events, which is estimated as 146.45° (4.08 Myr; see text). Only 18 of the 19 extinction cycles are represented because the phase angle of extinction # 1 cannot be computed because the corresponding 26 Myr CO_2 cycle is not complete (Figures 6–8). Abbreviations: CO_2, carbon dioxide; Myr, million years.

approach over peak analysis (Figure 10) is that it incorporates every datapoint in the extinction time series, which increases the sample size and leverages the statistical power of this dataset more fully.

The time period from 0 to 33 Mya resembled most closely today's planetary conditions, and is also the period of highest CO_2 data resolution. The regression of atmospheric CO_2 concentration on percent genus loss for this period (Figure 13a) has a Pearson correlation coefficient of $r = 0.8391$, discernibly different from zero at $p = 0.0006$. More than two–thirds of the variance in biodiversity loss during this time period is therefore explained by variance in atmospheric CO_2 concentration and conversely ($r^2 \times 100$, or $0.8391^2 \times 100 = 70.56\%$). The best-fit linear trendline for this dataset, established using the method of least squares, is described by the equation:

$$y = 0.0191x - 1.6496 \tag{1}$$

This equation is used below in this section to explore the possible impact of current CO_2 concentrations on biodiversity and energy policy.

Increasing the time period analyzed to 0–192 Mya and including the anomalous K-Pg extinction event (Figure 13b) reduces the correlation coefficient between atmospheric CO_2 concentration and percent genus loss to $r = 0.47$ ($p = 0.0001$). Eliminating data that bracket the K-Pg extinction and analyzing only older data (72–192 Mya; Figure 13c) yields a correlation coefficient of $r = 0.38$ ($p = 0.0016$). For the period 0–210 Mya, the corresponding $r = 0.36$ ($p = 0.002$). Therefore, with the exception of the time period bracketing the anomalous K-Pg extinction, atmospheric CO_2 concentration and percent genus loss are discernably and positively correlated over every time period evaluated in this study over the last 210 Myr.

The above regression analyses do not consider the demonstrated mean $\sim146.45°$ phase offset (~4.08 Myr on average) between CO_2 and biodiversity cycles. Moreover, two of the computed regressions incorporate the anomalous data from the K-Pg extinction (Figures 13b and 13d). When the percent genus loss dataset is phase lagged by ~4.08 Myr relative to the CO_2 cycle (the mean phase lag shown in Figure 9) and the regression analysis is repeated for the time period of 0–210 Ma, the correlation coefficient increases from $r = 0.360$ ($p = 0.002$; unshifted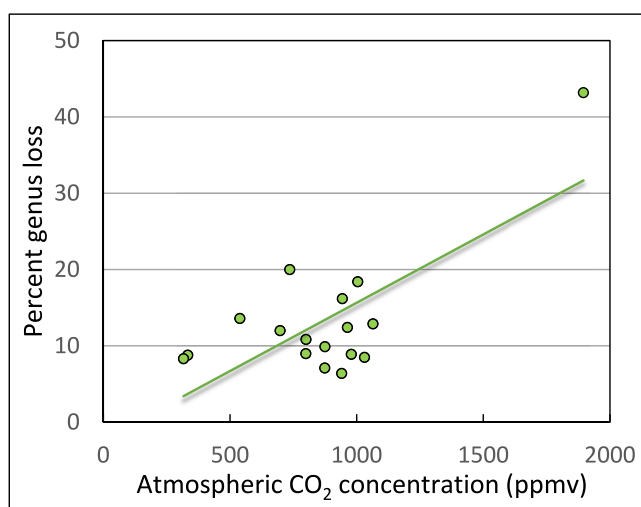 datasets, Figure 13d) to $r = 0.516$ ($p = 0.0002$; shifted datasets, Figure 14a). When the analysis of shifted datasets is conducted over the 0–210 time period but omits data from the anomalous K-Pg extinction (48–72 Mya), the correlation increases further to $r = 0.6252$ ($p < 0.0001$) (Figure 14b). This latter regression is used below in a sensitivity analysis of CO_2 reduction protocols, based on the corresponding best-fit (method of least squares) linear equation for the trendline:

$$y = 0.0061x + 3.8743 \tag{2}$$

These iterations of regression analyses highlight the impact of the two sources of variance introduced above, the phase shift between oscillatory CO_2 and percent genus loss, and the anomalous K-Pg data. Owing to this variance, some regressions and correlations between atmospheric CO_2 and percent genus loss computed here (Figures 13 and 14) are understated. The most accurate portrait of the CO/extinction relationship is the time period 0–33 Mya, where planetary conditions were most like today's (Figure 13a and Equation 1), and for the broader time period 0–210 Mya, where data resolution is highest for the Phanerozoic. Variance is reduced when CO_2/extinction data are phase shifted by ~4 Myr and when the anomalous K-Pg data are omitted (Figure 14b and Equation 2). These two regression models are therefore used below to explore the contemporary impact of CO_2 on biodiversity.
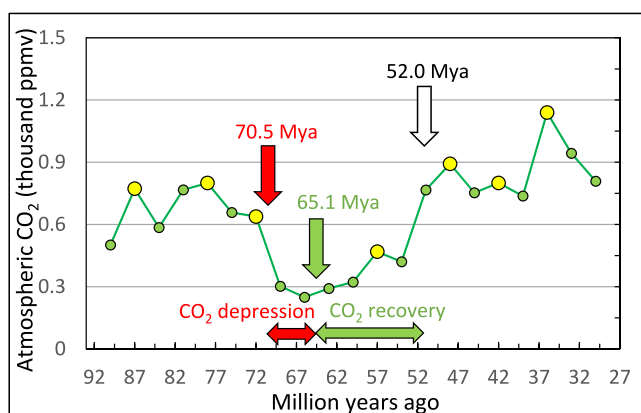
3.6. Mass Extinction Cycles and Global Temperature

Climate (temperature) change has frequently been invoked as a possible cause of past mass extinctions (e.g., Benton & Newell, 2014; Song et al., 2021; Vinós, 2022; Ward et al., 2000; Zhu et al., 2019). This hypothesis was tested

Figure 10. Scatterplot of peak atmospheric carbon dioxide (CO_2) concentration versus peak percent genus loss across extinction cycles of the last 210 million years. The Pearson product-moment correlation coefficient ($r = 0.72$) is discernible at $p = 0.0005$. The linear trendline was fitted by the method of least squares. Abbreviations: CO_2, carbon dioxide; ppmv, parts per million by volume.

by evaluating the relationship between atmospheric CO_2 concentration, mass extinctions, and proxies of global temperature, starting with the K-Pg extinction of the dinosaurs. Prior to the bolide impact that formed the Chicxulub crater ~66 Mya, long-term global temperature increased monotonically by ~3°C from 86 to 64 Mya (Figure 15). This increase in global temperature was accompanied by a decrease in the concentration of CO_2 in the atmosphere, from a high of 772 ppmv to a low of 291 ppmv (Figure 15). Atmospheric CO_2 and temperature appear negatively correlated over this time period, as reported previously for ~10% of time segments of the Phanerozoic Eon (W. J. Davis, 2017) and as confirmed below.

The apparent negative correlation between atmospheric CO_2 concentration and global temperature (Figure 15) is confirmed by calculation of the corresponding Pearson correlation coefficient. To compute this correlation coefficient, temperature was interpolated between datapoints in the temperature curve (Figure 15) to the times of datapoints in the CO_2 record. The correlation between atmospheric CO_2 concentration and interpolated global temperature proxies is discernible and negative ($r = -0.76$, $n = 8$, $p = 0.01$).

Progressive cross-correlation between global temperature and biodiversity loss over the last 210 Myr (Figure 16) shows a weak periodicity, with only 3 of 59 cross-correlation coefficients (10.3%) discernible at $p < 0.05$ (dashed red lines in Figure 16). As in the case of the K-Pg extinction, the cross-correlogram between temperature and percent genus loss over the whole of the fossil record provides evidence of at most a weak periodicity or coupling between biodiversity loss and long-term global temperature.
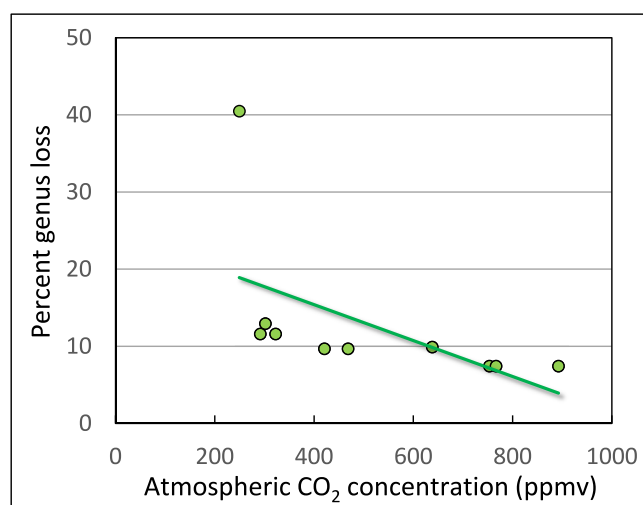
To further evaluate the relationship between long-term global temperature and biodiversity, percent genus loss was plotted against the corresponding long-term global temperature over the last 210 Myr (Figure 17). The correlation coefficient ($r = 0.03$) is not discernibly different from zero (non-directional t-test, $p = 0.80$), demonstrating the absence of a causal relationship. These results collectively require rejection of the hypothesis that long-term (Myr timescale) global temperature change caused extinction of biodiversity across the most highly resolved portion of the fossil record, the last 210 Myr. Short-term temperature spikes associated with transient volcanic activity ("hyperthermals"), however, are thought to have contributed to extinction events (Benton, 2018). Such brief episodes of global temperature change would not be detected at the sampling resolution available to this study.

3.7. Mass Extinction Cycles and Marginal Radiative Forcing by Carbon Dioxide

The most direct measure of the effect of CO_2 on temperature is marginal RF, the increment in temperature forcing associated with an increment in atmospheric CO_2 concentration. Marginal forcing associated with each CO_2 concentration datapoint was computed using MODTRAN (Section 2) and then correlated and progressively cross-correlated with percent genus loss. Across the last 210 million years, the Pearson product-moment correlation coefficient between biodiversity loss and marginal RF by CO_2 ($r = -0.001$) is not discernibly different from zero (non-directional t-test, $p = 0.99$) (Figure 18). Therefore, changes in marginal RF by atmospheric CO_2 did not cause extinction of biodiversity over the last 210 Myr.

This result is expected from the above finding that temperature is not discernibly correlated with genus loss. The progressive cross-correlation between marginal RF and biodiversity loss across the last 210 Myr (Figure 19) nonetheless shows strong periodicity and a well-formed cross-correlogram with

Figure 11. Time series showing the atmospheric concentration of carbon dioxide (CO_2) over the Cretaceous-Paleogene (K-Pg) mass extinction of the dinosaurs. Yellow datapoints are peaks in the 10 Myr cycle of atmospheric CO_2 concentration. Vertical arrows show the beginning of the carbon-cycle perturbation (red arrow), the onset of recovery (green arrow) and the time of full recovery (white arrow) 18.5 million years later. Horizontal double-headed arrows show the depression (red) and recovery (green) phases of the carbon cycle. The lines connecting datapoints in this time series are for visual clarity only and do not reflect the existence of real data between designated datapoints. Abbreviations: ppmv, parts per million by volume; Mya, million years ago; CO_2, carbon dioxide.

Figure 12. Scatterplot of peak atmospheric carbon dioxide (CO_2) concentration versus the corresponding percent genus loss over the time period bracketing the Cretaceous-Paleogene (K-Pg) extinction of the dinosaurs (45–75 million years ago). The Pearson correlation coefficient $r = -0.55$ (directional $p = 0.05$). The trendline was fitted by the method of least squares. Abbreviations: CO_2, carbon dioxide; ppmv, parts per million by volume.

numerous discernible ($p < 0.05$) correlation coefficients (12/49, or 24.5%). The long cycle evident in the periodogram repeats every 40–55 Myr, too short to qualify as the 63-Myr cycle shown by spectral analysis, but within the range of periodicities exhibited by geomagnetic reversals (Melott et al., 2018). The discernible periodicity of the cross-correlogram demonstrates both the cyclic variation of marginal RF and also its coupling with biodiversity loss. This finding, documented previously for marginal forcing in time series (Figure 11 in W. J. Davis, 2017), is likewise not surprising, inasmuch as marginal RF is computed from atmospheric CO_2 concentration, which as shown above is coupled strongly with biodiversity loss.

3.8. Carbon Dioxide Emission Reduction Scenarios

The above analysis of the fossil record shows that atmospheric CO_2 concentration is discernibly correlated with biodiversity loss over at least the last 210 Myr. Using the regression of CO_2 concentration on percent genus loss over the most recent 33 Myr of the fossil record as a guide (Figure 13a), the best-fit trendline (Equation 1) shows that today's atmospheric concentration of CO_2, ~421 ppmv, is equivalent to a 6.39% genus loss. This loss approaches the smallest percent genus loss of natural mass extinctions, 6.40%, corresponding to extinction event # 10, 132.5 Mya (Figure 4), and therefore qualifies within likely error limits as an extinction event as operationally defined here. The discovery of significant genus loss in the fossil record associated with the current atmospheric concentration of CO_2 implies that contemporary biodiversity has declined by the same percentage and invites the question of how much reduction in contemporary anthropogenic CO_2 emissions is required to reverse the inferred ongoing human-induced extinction event.
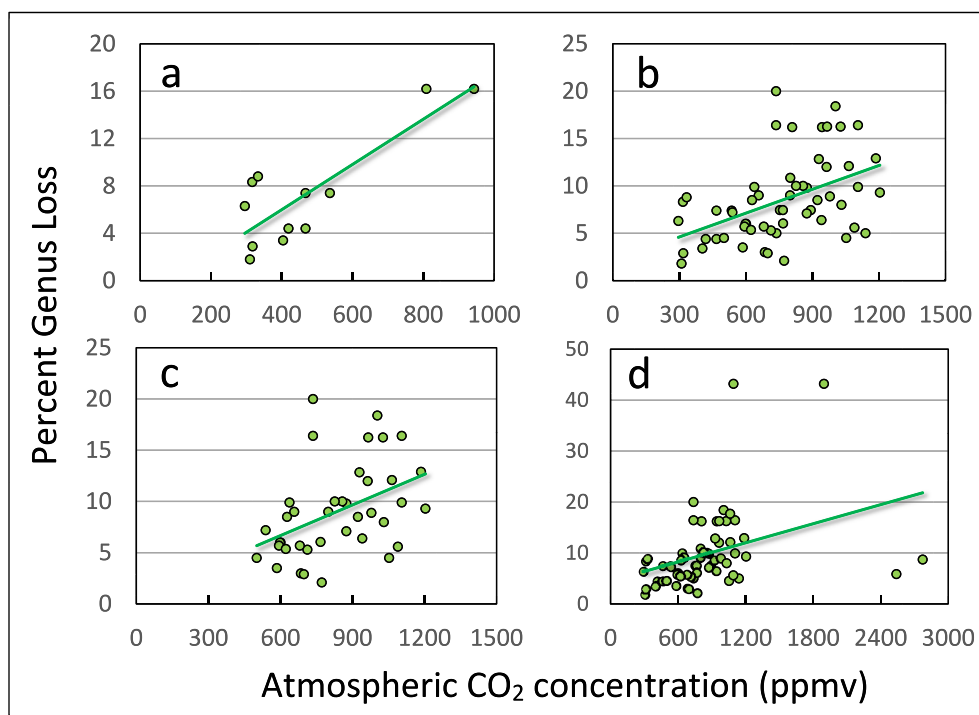
Figure 13. Regression of atmospheric CO_2 concentration on percent genus loss for different time periods of the Phanerozoic Eon. (a) 0–33 million years ago (Mya; Pearson correlation coefficient $r = 0.8391$, $p = 0.0006$); (b) 0–192 Mya ($r = 0.470$, $p = 0.0001$); (c) 72–192 Mya ($r = 0.3760$, $p = 0.0016$); (d) 0–210 Mya ($r = 0.360$, $p = 0.002$). Trendlines were fitted by the method of least squares. Abbreviations: ppmv, parts per million by volume; CO_2, carbon dioxide.
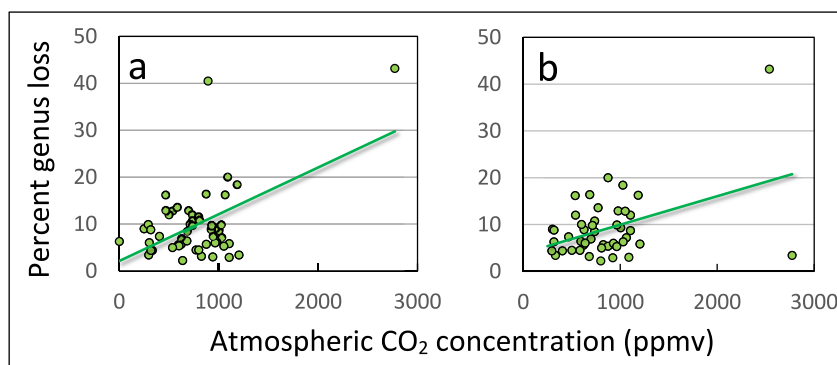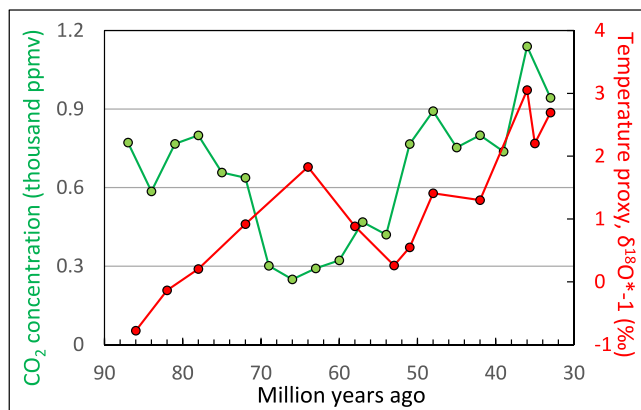
Figure 14. Regression of atmospheric CO_2 concentration on percent genus loss for the period 0–210 million years ago (Mya). In both graphs, percent genus loss is lagged 4.08 million years (Myr) relative to atmospheric CO_2 concentration (mean phase shift from Figure 9). (a) Data from K-Pg extinction time period included (Pearson correlation coefficient $r = 0.516$, $p = 0.0002$); (b) data from K-Pg extinction time period excluded ($r = 0.6252$, $p < 0.0001$). Abbreviations: CO_2, carbon dioxide; ppmv, parts per million by volume.

To address this question several emission-reduction scenarios that could stem the current loss of biodiversity were evaluated. For this purpose it was assumed conservatively that atmospheric CO_2 concentration will increase by 2.0 ppmv year^{-1} (yr^{-1}) based on ground observations at Mauna Loa in the last decade (annual increase of 2.4 ppmv yr^{-1}; NOAA, 2020, 2021), satellite measurements of atmospheric CO_2 from 2003 to 2020 (1.9 ± 0.4 ppmv yr^{-1}; Gier et al., 2020), and model projections for the period 2003–2020 (CanESM2 model, 2.4 ± 0.4 ppmv yr^{-1}; CMIP6 model, 2.3 ± 0.03 ppmv yr^{-1}; Gier et al., 2020). The annual increase in atmospheric CO_2 concentration, assumed here as 2 ppmv, is caused almost entirely by anthropogenic emissions of CO_2 (IPCC, 2001, 2021, 2022). Abatement of anthropogenic emissions therefore requires reduction of the current annual rise in atmospheric CO_2 concentration to zero. On this basis the effects on biodiversity loss of reducing the annual anthropogenic CO_2 emission from 2.0 ppmv yr^{-1} to zero were computed in integral steps ranging from 1% to 10% per year, using Equation 1 as the regression model.
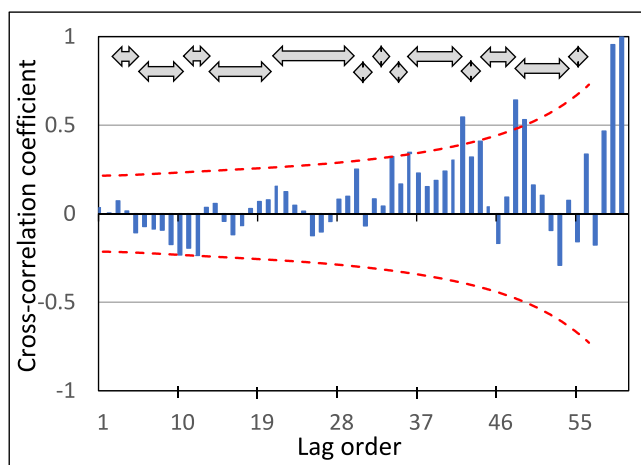
This analysis assumes that CO_2 emission reductions begin in the year 2023, and that these annual reductions continue until net anthropogenic emissions reach zero ("CO_2 stabilization"). At that time the concentration of CO_2 in the atmosphere is expected to begin a long decline from the CO_2 stabilization plateau. The consequent reversal in CO_2 sink/source dynamics is expected to reduce atmospheric CO_2 concentration over decades to centuries to the historical interstadial concentration of ~280–300 ppmv. There it would in principle remain until the onset of the next GIA, projected for 68–108 Kyr into the future based on past periodicities. The analysis assumes that the efficacy of natural oceanic and terrestrial sinks for CO_2 remains unchanged, that is, that these sinks continue to operate with the same efficiency as today. This assumption may be unlikely as the ocean equilibrates to higher CO_2 concentrations and natural sinks become more saturated (Jiang et al., 2019), in which case this analysis may overstate proportionally the efficacy of reduced emissions as computed here.


Figure 15. Time series showing the atmospheric concentration of carbon dioxide (CO_2, green curve) and simultaneous temperature proxy (red curve) over the Cretaceous-Paleogene (K-Pg) mass extinction. The lines connecting datapoints in this time series are for visual clarity only and do not reflect the existence of real data between designated datapoints. Abbreviations: CO_2, carbon dioxide; ppmv, parts per million by volume; $\delta^{18}O * -1$ (‰), delta-O-18 in parts per thousand, ‰, multiplied by −1 (see text).

If the highest rate of emission reductions considered here, 10% yr^{-1}, were implemented starting in the year 2023, 100% of anthropogenic CO_2 emissions would be eliminated in 10 years. The concentration of CO_2 in the atmosphere would stabilize in the year 2032 at 432.0 ppmv, computed arithmetically by adding to the CO_2 concentration at the beginning of the sequence (421 ppmv) the projected 2 ppmv rise per year as reduced every year after the first by 10%. This sum is then entered into Equation 1, yielding the percentage genus loss at CO_2 stabilization of 6.60% (Figure 20, left-most datapoint), marginally greater than the loss already committed by anthropogenic emissions (6.39%; see above) and greater than the smallest extinction event on record, 6.4% genus loss (# 10, 132.5 Mya, Figure 4). A 10% annual CO_2 reduction

Figure 16. Progressive cross-correlogram of global temperature versus percent genus loss for the time period 210-0 million years ago. Gray double-headed arrows demarcate visible cycles in the cross correlations that correspond to a weak and poorly-organized periodicity that seldom reaches significance at $p < 0.05$. Lag order here corresponds to a time shift of 3.50 Myr. Dashed red lines show the 95% confidence limits for the discernibility of correlation coefficients.

scenario is economically infeasible, however, because it would require large-scale retirement of valuable capital stock associated with the fossil-fuel infrastructure long before it reaches its functional lifespan of 30–50 years. Although unrealistic in practice, the 10% yr^{-1} emission reduction scenario is included here to anchor mathematically one extreme of the range of scenarios considered (Figure 20).

At the other extreme, the lowest CO_2 emission-reduction rate considered here is 1% yr^{-1}. Under this reduction scenario, anthropogenic emissions would be eliminated in one century, but the slower rate of emission reductions would raise the eventual maximum concentration of CO_2 in the atmosphere to a stabilization peak of 522.0 ppmv. The corresponding percent biodiversity loss calculated from Equation 1 is 8.32%, within the range of the percent genus loss recorded in the fossil record during the two most recent mass extinctions (8.8% and 8.3%; Figure 1) and near the mean of the smallest nine extinction events of the last 210 Myr, 8.3% genus loss. A one-century transition to a carbon-neutral economy is more feasible economically because it allows more time to replace fossil-fuel capital at the end of its natural lifetime with new capital appropriate to a renewable energy economy. Such a long delay to CO_2 stabilization would incur a disproportionate risk to global biodiversity, however, resulting in atmospheric concentrations of CO_2, near the mean genus loss of the smallest nine mass extinctions of the last 210 Myr, 8.3%.

The genus loss curve in Figure 20 shows that at higher rates of annual emission reductions (left side of the curve), incremental or marginal reduction in biodiversity loss—the "benefit" in this cost-benefit comparison—increases slowly as annual emission reductions decline. At lower rates of annual emission reductions (right side of the curve), the marginal benefit goes up faster as emission reduction rate declines. These qualitative observations are quantified by the marginal benefit curve, constructed by subtracting the percent genus loss associated with each datapoint in Figure 20 from the percent genus loss associated with the following datapoint in the sequence (a "difference" curve; Figure 21).
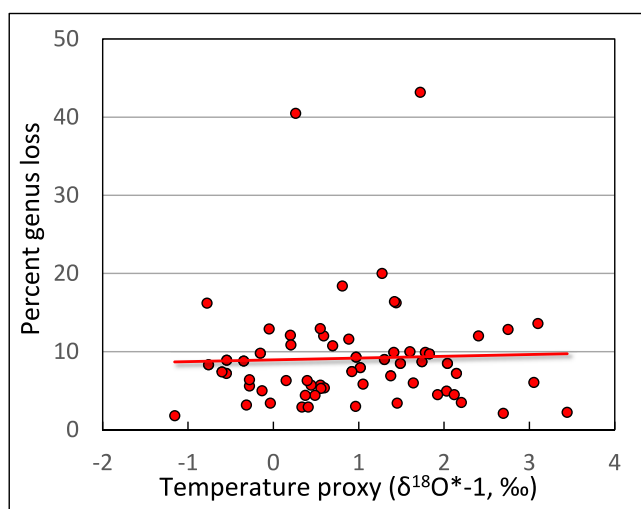
Figure 17. Scatterplot of a temperature proxy versus percent genus loss for the last 210 million years. The red trendline is the best-fit (method of least squares) linear function. The Pearson product-moment correlation coefficient ($r = 0.03$) is not discernibly different from zero ($p = 0.80$). Abbreviation: $\delta^{18}O * -1$ (‰), delta-O-18, the ratio of stable isotopes oxygen-18 (^{18}O) and oxygen-16 (^{16}O) in parts per thousand (‰), multiplied by −1 (see text).

The marginal benefit (decline in percent genus loss) obtained by reducing emission cuts from 10% to 9% yr^{-1} is 0.02%, and from 2% to 1% yr^{-1}, 1.89% (Figure 21). The marginal benefit of CO_2 emission-reduction protocols is therefore two orders of magnitude greater for smaller emission cuts spread over longer periods of time. Optimizing the cost/benefit ratio of emissions-reduction protocols requires operating on the steeper portions of the marginal benefit curve, that is, adopting slower emission cuts that are economically and socially less disruptive, yet achieve higher marginal extinction reduction benefits—in the range of 2%–3% CO_2 emission reduction per year.
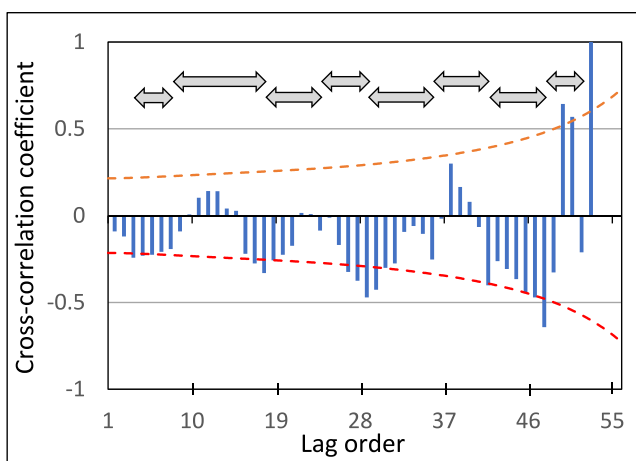
The above cost-benefit analysis is based on the relationship between atmospheric CO_2 and extinction cycles over the last 33 Myr, when conditions on Earth were most similar to today. The same analysis was done for the time period 0–210 Mya after correcting for the demonstrated phase lag by using phase-shifted data, and excluding the anomalous K-Pg event (Figure 14b). Equation 2 was in this case used as the regression model. The computed percent genus loss associated with today's atmospheric concentration using the 0–210 Myr regression model, 6.35%, is nearly unchanged from the value based on the 0–33 Myr dataset, 6.39%. The estimate of current biodiversity loss is therefore relatively insensitive to the use of different extinction curves. All projected genus losses for both regressions are similar (within 10%) for scenarios of 10%–3% emission reductions annually (Figure 22). The primary difference between the regression models appears at lower percent emission
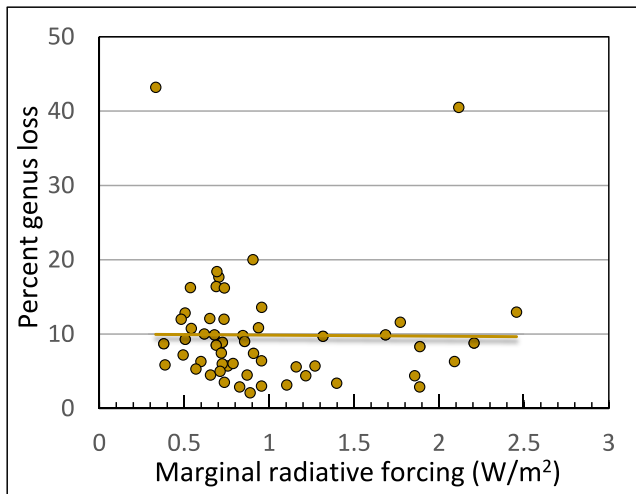
Figure 18. Scatterplot of marginal radiative forcing versus percent genus loss for the last 210 million years. The trendline is the best-fit linear function (method of least squares). The Pearson product-moment correlation coefficient ($r = -0.001$) is not discernibly different from zero ($p = 0.80$). Abbreviation: W/m^2, Watts per square meter at the top of the troposphere computed from observed proxy CO$_2$ concentration using MODTRAN.

cuts spread over longer time periods, where computed values for projected genus loss are 10%–15% lower (Figure 22; cf. with Figure 20).
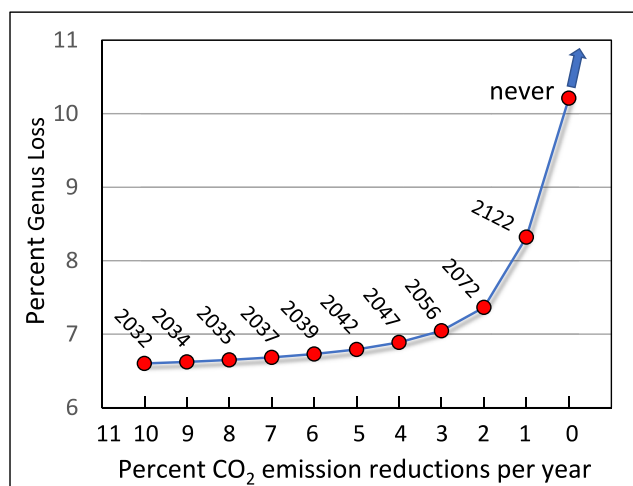
Comparison of the marginal benefit curves for the two regression models (Figures 21 and 23) gives a similar result. Marginal benefit is similar for larger cuts spread over shorter time periods (datapoints from 10% to 3% emission cuts per year), but marginal benefits at lower percent emission cuts (2%−1% yr^{-1}) are up to 25% greater for the first regression model based on the fossil record of 0–33 Mya (cf. Figure 23 with Figure 21). This rudimentary sensitivity analysis shows that outcomes are generally similar with both regression models, that is, conclusions are relatively insensitive to the regression model used, but moderately larger marginal benefits are realized when percent genus loss is more highly correlated with atmospheric CO$_2$ concentration ($r = 0.84$ vs. 0.63 for regression models # 1 and # 2, respectively), as expected.

4. Discussion

This study uses the fossil record to estimate the potential risk to contemporary biodiversity of anthropogenic carbon dioxide (CO$_2$) emissions and consequent ocean acidification. The main finding is that mass extinctions of the past oscillate at the same periodicity as the multimillion-year atmospheric CO$_2$ cycle reported previously (W. J. Davis, 2017). Percent genus loss in the fossil record is discernibly correlated with atmospheric CO$_2$, concentration, but not with long-term global temperature ("climate") nor with marginal RF of temperature by atmospheric CO$_2$. Therefore, increased atmospheric CO$_2$ concentration and consequent ocean acidification is a plausible kill mechanism of most past mass extinctions, while long-term global temperature (climate) change and marginal RF by CO$_2$ are excluded as possible causes of past mass extinctions.

The regression of past CO$_2$ concentration on percent genus loss as registered in the marine fossil record provides a quantitative metric for estimating the contemporary effects of anthropogenic CO$_2$ emissions on biodiversity. The current atmospheric CO$_2$ concentration (∼421 ppmv) is associated in the fossil record with a 6.39% loss of biodiversity (computed from Equation 1). This projected contemporary genus loss approaches the 6.40% genus loss of the smallest mass extinction event identified here (# 10, 132.5 Mya, Figure 4), and implies that present anthropogenic emissions are now causing the extinction of marine life. This ongoing loss of biodiversity is increasing rapidly in direct proportion to the annual increase in atmospheric CO$_2$ concentration.

Projections of this approach into the immediate future portend an imminent rapid collapse in biodiversity that is comparable in size and global scope to natural mass extinctions of the past. The main differences are the timing and source of CO$_2$ emissions. Past natural mass extinctions unfolded incrementally on timescales of millions of years and all occurred before the appearance on Earth of humans. The current anthropogenic extinction is developing orders of magnitude faster, over a time period of less than three centuries, and is caused exclusively by humans.

Because human activities are responsible for nearly all of the increased atmospheric CO$_2$ registered since 1770 (IPCC, 2021), the only way to avoid an anthropogenic mass extinction is to eliminate net anthropogenic emissions of CO$_2$. This study evaluates a range of CO$_2$ emission-reduction scenarios in light of the CO$_2$/extinction relationship represented in the fossil record. The main policy finding is that the optimal path to avoiding an anthropogenic mass extinction is emplacement of a carbon-neutral economy over the next 50 years by means of a 2% annual reduction in net anthropogenic emissions

Figure 19. Progressive cross-correlation between marginal radiative forcing by atmospheric carbon dioxide (CO$_2$) and percent genus loss for the time period 210-0 million years (Myr) before present. Lag order here corresponds to a time interval of 3.89 Myr. Red dashed lines show the $p = 0.05$ probability level for the discernibility of correlation coefficients. Gray double-headed arrows demarcate visible cycles in the cross correlations that have a mean periodicity of 26.4 Myr.

Figure 20. The effect of the rate of emission reductions on biodiversity loss. The year above each datapoint indicates the time that atmospheric CO_2 concentration will stabilize at the level of genus loss indicated on the ordinate. This graph is based on the regression of CO_2 on percent genus loss from 0 to 33 million years ago (Mya) (Figure 13a and Equation 1). Abbreviation: CO_2, carbon dioxide.

starting immediately. This conclusion was developed using the fossil record of mass extinction cycles to derive insights for current energy and economic policy, and Section 4 follows the same logical sequence.

4.1. The Number and Frequency of Past Mass Extinction Cycles

The first scientific study of mass extinctions in the modern era (Newell, 1952) identified five major ("canonical") mass extinctions of the past. These global collapses of biodiversity were among the largest, fastest and geographically broadest of known past biodiversity drawdowns. Several previous mass extinctions were larger, however, and many more periodic peaks in genus loss have been termed mass extinctions even though they were smaller than the canonical five (Bambach, 2006; Melott & Bambach, 2014; J. J. Sepkoski, 2002). Bambach (2006) applied diverse sorting protocols to the J. J. Sepkoski (1986, 2002) database to qualify 18 peaks in percent genus loss as mass extinctions. Using the same database, Kidder and Worsley (2010) documented 23 mass extinction events, while Melott and Bambach (2014) identified 25. In earlier studies, Hallam and Wignall (1997) found 26 mass extinctions, while Walliser (1996) recognized 61. The most extreme application of the Sepkoski definition of a mass extinction, namely, any detectable increase in biodiversity loss (Section 2), qualifies 78 increases in biodiversity loss in the fossil record as mass extinction events (Figure 1). Erlykin et al. (2017) reported "163 genus extinction events" (ibid., p. 160) based on the datasets used by Bambach, perhaps conflating extinction events with the sample size of this database ($n = 163$).

The variation in estimates of the number of past mass extinctions results largely from the absence of a common definition. When each local peak in biodiversity loss on a Myr-timescale is considered an extinction event, as proposed by Bambach (2006) and as implemented here (Section 2), there have been 50 extinction events over the past 534 million years (Figure 4). This count includes the five canonical mass extinctions, 20 additional and previously-recognized smaller extinction events (Melott & Bambach, 2014), and 25 additional and generally still smaller peaks in genus loss identified here that were previously classified as "sub-extinction stages" (Bambach, 2006; Melott & Bambach, 2014).

The identification here of 50 extinction cycles over a period of 534 Myr implies a mean periodicity of 10.68 Myr, similar within likely error limits to the lowest significant periodicity demonstrated previously for the extinction record by spectral density analysis, ~10 Myr (ibid.) and within the 10–15 Myr periodicity range reported for atmospheric CO_2 concentration (W. J. Davis, 2017). The definition of a mass extinction adopted here—a peak in genus loss flanked by lesser values—therefore resolves the previous inconsistency between spectral power analysis and the estimated number and frequency of past mass extinction events.

4.2. The Temporal Structure of Past Mass Extinctions

The early nineteenth century French naturalist Georges Cuvier interpreted the evolution of the Earth as a series of singular, instantaneous (on geologic time scales) global catastrophes (Rudwick, 1997; D. Sepkoski, 2020). The earliest modern investigators of mass extinctions conceived the biodiversity collapses they observed similarly, as punctate evolutionary crises that recur over time (e.g., Newell, 1952, 1962, 1963, 1967; Schindewolf, 1954, 1963; Knoll, 1984). This "catastrophe theory" of mass extinctions, as opposed to
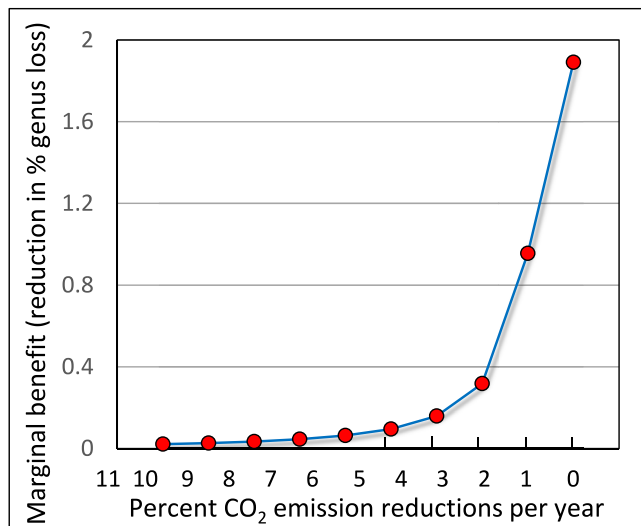
Figure 21. Marginal benefit curve. Shown is the incremental increase in benefit (marginal reduction in biodiversity loss) versus annual reduction in anthropogenic carbon dioxide (CO_2) emissions. The curve was made by subtracting each datapoint of percent loss from the subsequent datapoint in Figure 20. Disproportionately greater marginal benefit (reduction in biodiversity loss) is achieved at lower rates of emission reductions spread over longer time periods (right side of graph). This graph is based on analysis of fossil data from 0 to 33 million years ago (Mya) (Figure 13a and Equation 1). Abbreviation: CO_2, carbon dioxide.
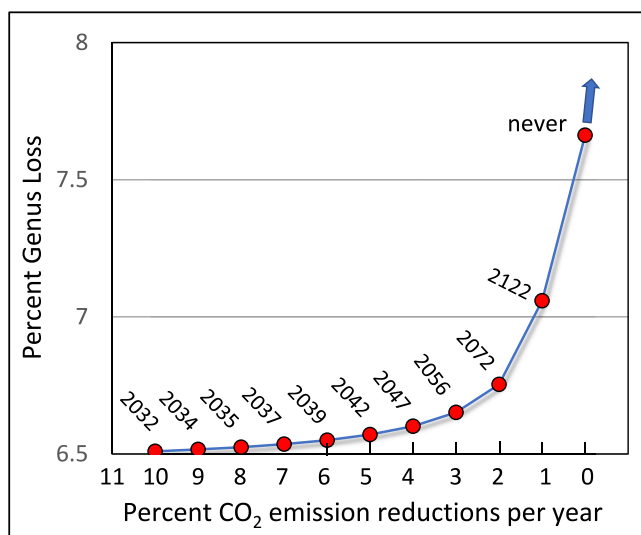
Figure 22. Sensitivity analysis of regression model to estimate percent genus loss. As in Figure 20, except this graph is based on Equation 2 covering the period 0–210 years ago (Mya) (Figure 14b). Cf. with Figure 20. Abbreviation: CO_2, carbon dioxide.

the "incrementalism" espoused by Darwin and others, was revived in the form of "neocatastrophism" through studies of the Cretaceous-Paleogene (K-Pg) extinction of the dinosaurs (Schindewolf, 1963; D. Sepkoski, 2020). The generally-accepted cause of the K-Pg extinction was the collision of the Earth with an extraterrestrial body followed by an "impact winter" that blocked sunlight, truncated photosynthesis, and obliterated most life on Earth (L. W. Alvarez et al., 1980).

As shown here, however, and as recognized by the same authors (L. Alvarez et al., 1984; Hut et al., 1987), the K-Pg extinction event was characterized by steady genus loss 20 Myr prior to the bolide impact ~66 Mya (Figure 1). The recovery of genera required an equally long time of ~20 Myr. At the same time, the long-term carbon cycle was deeply perturbed, as evidenced by a precipitous drop in atmospheric CO_2 concentration starting ~5 Myr before the K-Pg extinction event at ~66 Mya, with full recovery ~20 Myr later (Figure 11). The long (Myr) build-up and decay of biodiversity loss that flanked the extinction event at ~66 Mya suggests that "The paleontological record…bears witness to terminal-Cretaceous extinctions on two time scales: a slow decline unrelated to the impact and a sharp truncation synchronous with and probably caused by the impact." (L. Alvarez et al., 1984, p. 1135).

These studies provided among the early clues that the extinction record might be continuous (incremental) rather than, or in addition to, episodic (catastrophic). In a then-controversial departure from the paradigm of catastrophism, and following Newell's (1952) earlier proposal, Raup and Sepkoski (1984) found that the fossil record exhibits underlying periodicities. The same paper also marks one of the earliest in which extinction events were considered more common in paleohistory than the canonical five identified by Newell (1952). Following this logic, Foote (2005) concluded, using the J. J. Sepkoski (1986) database, that extinctions at the genus level are pulsed, that is, periodic, although still best explained as a single episode per extinction cycle (Foote, 2005, p. 15). The present study extends and refines this concept with the finding that genus loss is continuous within each extinction cycle to its peak, defined as the mass extinction event, whereupon genus recovery begins and is similarly continuous over millions of years (Figure 5).
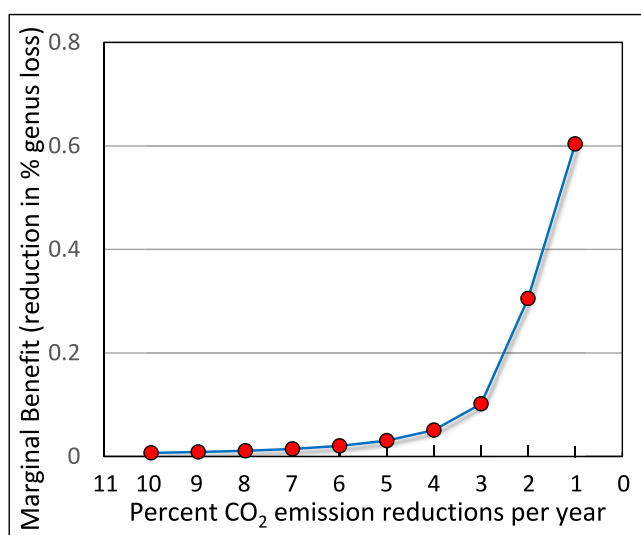
Figure 23. Sensitivity analysis of marginal benefit curve. As in Figure 21, except this graph is based on analysis of fossil data from 0 to 210 Mya, shifted by 4.08 Myr to align phases of the respective cycles and excluding data bracketing the K-Pg extinction (Figure 14b and Equation 2). Abbreviation: CO_2, carbon dioxide.

The bolide impact that marked the end-Cretaceous extinction was by most measures "catastrophic." However, as noted, biodiversity had been falling steadily for millions of years prior to the generally-accepted extinction event at ~66 Mya as "the result of gradual processes and not of a single event." (Archibald & Clemens, 1982). As found here, all five of the identified canonical mass extinctions follow the same temporal rise-fall pattern, as do the remaining 20 previously-identified mass extinctions (Melott & Bambach, 2014), the 25 newly-identified extinction events proposed here, and the collective total of 50 extinction events recognized here (Figure 5). This study therefore shows that a cyclic build-up and decline of biodiversity loss on million-year timescales is a universal property of past mass extinction cycles.

Mass extinctions were therefore not single, catastrophic events that occurred randomly over deep time. Rather, their temporal structure shows that they are regular occurrences in paleohistory, each of which builds gradually on Myr timescales to a peak that is defined as the extinction event, and then decays over a comparable Myr time period. This discovery, presaged by L. Alvarez et al. (1984) for the K-Pg extinction, is confirmed here for all mass extinction events over the last 534 Myr. This interpretation implies that the underlying causes of mass extinctions are continuous rather than discrete processes (Archibald & Clemens, 1982), which in turn constrains the "kill mechanism" to candidates that satisfy this key continuity criterion. The historic polarization of the debate between Cuvier's catastrophism (revolutionary change) and

Darwin's incrementalism (evolutionary change) therefore has a straightforward resolution: both are valid. Mass extinctions were punctuated by "catastrophic" global changes, and were periodic across deep time and incremental in their development within the million-year cycles in which they unfold.

4.3. The Cretaceous-Paleogene (K-Pg) Extinction of the Dinosaurs

The end-Cretaceous (K-Pg) extinction is the most widely-cited example of the catastrophe theory of mass extinctions and one of the most intensively investigated extinction events. The K-Pg extinction is characterized stratigraphically by a worldwide sedimentary layer of bentonite clay enriched in iridium, a metal that is relatively diffuse in the Earth's crust but concentrated in asteroids (Schulte, 2010). On this basis L. W. Alvarez et al. (1980) proposed that the K-Pg extinction resulted from the impact on Earth ~66 Mya of a comet/asteroid, or bolide, estimated to be 6–14 km in diameter. This hypothesis was strengthened by the discovery of the resulting Chicxulub impact crater (Hildebrand et al., 1991) and documentation of a brief (Kyr) "impact winter" that reduced regional sea surface temperatures for a few Kyr following the impact (Vellekoop et al., 2014).

Over several hundred millennia prior to the K-Pg extinction event at ~66 Mya, however, the Earth underwent repeated basalt floods in the form of Large Igneous Provinces (LIPs) associated with corresponding spikes in global temperature ("hyperthermals"). These events were followed by increased atmospheric CO_2, ocean acidification, anoxia, and biodiversity loss (Benton, 2018; Bond & Wignall, 2014; Ernst & Youbi. 2017; Keller et al., 2020). These studies suggest that "Deccan-induced hyperthermal and ocean acidification led to the KPB [K-Pg] mass extinction" (Keller et al., 2020). The bolide impact that formed the Chicxulub crater triggered a state shift in Deccan (Indian) volcanism on the other side of the globe (Renne et al., 2015; Richards et al., 2015), providing the missing link between the impact of extraterrestrial bodies and mass extinction through accelerated plate tectonics that generate LIPs, vent CO_2 to the atmosphere, and acidify the global ocean. Ocean acidification was therefore a central contributor to the K-Pg extinction.

The present study shows that the K-Pg extinction is nonetheless unique among all mass extinction events in at least three respects. First, its cycle duration, ~40 Myr, is the longest by an order of magnitude of any other mass extinction recorded over the last 534 Myr (Figure 5). Second, over the best-resolved portion of the Phanerozoic Eon, the last 210 Myr, the percent genus loss during the K-Pg extinction was exceptional, smaller only than the T-J extinction, and yet the concentration of CO_2 in the atmosphere as measured by standard proxies was the lowest on record for any mass extinction event, 249 ppmv—less even than normal interstadial concentration of ~280–300 ppmv (e.g., Sigman & Boyle, 2000), although the error variance of this concentration value is unknown. Third, and related, the K-Pg mass extinction is one of the few that occurred not near the peak of the long-term (26 Myr) CO_2 cycle, but rather near its apparent trough, when CO_2 concentration is averaged on a Myr timescale (Figure 11). This trough lasted 18.5 Myr, the longest and deepest depression of atmospheric CO_2 concentration of any extinction cycle of the last 534 Myr.

This study therefore shows that the K-Pg mass extinction was either initiated, mediated, or at least accompanied by a multi-million year perturbation of the carbon cycle, manifest as depressed atmospheric CO_2 concentration. Recent studies suggest that the diversity of dinosaur species also began its long decline 10 Myr prior to the bolide impact at ~66 Ma (Condamine et al., 2021), as reflected for all marine genera in Figure 1. Depression of long-term global atmospheric CO_2 concentration began millions of years earlier and lasted for up to several million years after the accepted mass extinction date at ~66 Myr. These findings are nonetheless consistent with the conclusion that "Perturbation of the atmospheric carbon cycle…likely lasted less than 5,000 years, exhibiting a recovery time scale two to three orders of magnitude shorter than that of the major ocean basins." (Renne et al., 2013, p. 684), inasmuch as the present study could not distinguish such short, intense fluctuations of the carbon cycle because of its limits on sampling frequency.

Modeling studies suggest that the impact of a large bolide would launch particulate matter into the atmosphere to block sunlight from reaching the Earth's surface and initiate an "impact winter" similar to the postulated "nuclear winter" projected to result from atomic warfare (e.g., Robock et al., 2007). Modeling of the K-Pg extinction event, however, suggests that the consequent blockage of solar insolation would persist for decades to centuries (Harrison et al., 2022) and therefore was not alone responsible for the multimillion-year depression of atmospheric CO_2. Evidence increasingly suggests that the K-Pg extinction may have had multiple simultaneous causes, including not only the decisive bolide impact ~66 Mya followed by a brief impact winter, but also earlier enhanced volcanic

activity, emplacement of LIPs, ocean acidification and corresponding anoxia, and broad depression of biological productivity from depressed photosynthesis, all expressed on multi-million-year timescales (Keller et al., 2020). Such multiple causation of extinction events probably characterized all past mass extinctions without, however, detracting from the primacy of atmospheric CO_2 and consequent ocean acidification as the most direct, pervasive and immediate kill mechanism of most mass extinctions.

The abrupt decline in atmospheric CO_2 starting ∼5 Myr prior to the K-Pg extinction is paradoxical, however, for three reasons. First, average global temperature soared by 3°C over this same time period (Figure 12; see below). For comparison, the contemporary global warming episode has increased global temperature by 1.1°C (NASA, 2022), although over a much shorter time period. Since CO_2 is less soluble in warmer ocean water, a 3°C temperature increase would have vented gigatons (GTs) of CO_2 from the ocean to the atmosphere at the same time the fossil record paradoxically shows a precipitous drop in long-term atmospheric CO_2 concentration. Second, simultaneous widespread combustion of the Earth's forests and subterranean fossil fuel stores triggered by collision with a massive bolide would have degassed additional GTs of CO_2 into the atmosphere. Third, subterranean CO_2 released from a fractured crust as a consequence of enhanced volcanic activity in the form of LIPs vented additional GTs of CO_2 to the atmosphere over a time period that nonetheless witnessed long-term *depression* of atmospheric CO_2 concentration.

These apparent paradoxes raise three questions about the K-Pg extinction and the related carbon cycle. Why did biodiversity loss begin in earnest 20 Myr before the bolide impact that is generally thought to have caused the extinction event? Why did the concentration of CO_2 in the Earth's atmosphere decline so radically starting nearly 5 million years before that catastrophic collision (Figure 11)? And why did full recovery of "normal" (pre-extinction) CO_2 baselines and resumption of cyclic CO_2 pulsing require yet an additional 14 Myr after the K-Pg extinction event at ∼66 Mya (Figure 11)? Answers may include long-term bombardment of the Earth's surface by a string of bolide showers and consequent stepwise changes in biodiversity abundance (L. W. Alvarez et al., 1980; L. Alvarez et al., 1984; L. Alvarez & Muller, 1984; Hut et al., 1987) accompanied by a more or less continuous and increasing "impact winter" that lasted for millions of years.

Alternatively, rapid changes in CO_2 and temperature may have occurred that are not detectable at the sampling frequencies employed in the present study owing to Nyquist-Shannon sampling frequency threshold limit of two samples per cycle. Periodic, stepwise venting of CO_2 on millennial-timescales could explain steadily-increasing biodiversity loss prior to the ∼66-Mya extinction event (Hut et al., 1987), and any such transient signals would be undetectable at the comparatively coarse data resolution that characterizes this study.

4.4. Atmospheric Carbon Dioxide Concentration and Mass Extinction Cycles

A plethora of studies has established atmospheric CO_2 and consequent ocean acidification and anoxia as a dominant proximal cause of past mass extinctions (e.g., Beauchamp & Grasby, 2012; Bond & Grasby, 2017a, 2017b; Clapham & Payne, 2011; Clapham & Renne, 2019; Clarkson et al., 2015; Fox et al., 2022; Greene et al., 2012; N. Hautmann, 2004; M. Hautmann, Benton, et al., 2008, M. Hautmann, Stiller, et al., 2008; Heydari et al., 2013; Hinojosa et al., 2012; Jurikova et al., 2020; Larina et al., 2021; Martindale et al., 2012; Montenegro et al., 2011; Payne et al., 2007). The resulting acidification of the ocean exterminated global phytoplankton populations (e.g., Fox et al., 2022), causing the collapse of primary production (Fox et al., 2022; Twitchett, 2006) and inducing widespread oceanic and terrestrial anoxia and the consequent mass extinction of species (e.g., Bond et al., 2004; Bond & Wignall, 2010; Brenchley et al., 1994, 2001; Buggisch, 1991; Clapham & Renne, 2019; Fox et al., 2022; Grice et al., 2005; House, 1985; Isozaki, 1997; Shen et al., 2016; Wang et al., 2016; Wignall & Hallam, 1992; Wignall & Twitchett, 1996). Marine anoxia caused by the collapse of phytoplankton populations and the resulting decline in primary production of oxygen teleconnected quickly through the atmosphere to contribute to near-simultaneous (on geological timescales) terrestrial anoxia and coupled extinction on land (Algeo et al., 2011; Beauchamp & Grasby, 2012; Dal Corso et al., 2022; Grice et al., 2005; Kidder & Worsley, 2010).

The present study supplements previous work (W. J. Davis, 2017) showing that atmospheric CO_2 concentration varies cyclically with the extinction cycle, and shows further that the CO_2 cycle leads the extinction cycle by ∼4 Myr. This demonstrated phase relationship is consistent with the hypothesis that increasing atmospheric CO_2 is the immediate cause of most past mass extinction events. On this basis the possible role of CO_2 in mass extinctions is quantified over the past 210 Myr, where data resolution is highest, and during which period the most recent 19 extinction events occurred. With notable exceptions, including most prominently the K-Pg extinction

of the dinosaurs discussed above, atmospheric CO_2 concentration is discernibly correlated ($r \cong 0.36$–0.84) with percent genus loss over the last 210 Myr, consistent with the hypothesis that atmospheric CO_2 and consequent acidification of the ocean and widespread anoxia was the immediate kill mechanism of past mass extinctions. A full understanding of the extinction cycle requires unraveling the causal chain between CO_2 degassing and precursor events that represent the ultimate causes of mass extinctions, as attempted below.

The earliest students of the fossil record observed that extinction events decline in amplitude over the Phanerozoic Eon. Similarly, the concentration of CO_2 in Earth's atmosphere declined over the time period for which data are available, the last 425 million years (W. J. Davis, 2017). The decline in atmospheric CO_2 concentration is attributable in part to its greater solubility in a steadily-cooling ocean, and in part to the reduced size and geographical extent of LIPs as the mantle cooled. Recent studies show that mantle cooling began abruptly at the beginning of the Cryogenian Period (Chen et al., 2022) and continued by an additional 50–70°C during the last 540 Myr (Condie et al., 2016; Herzberg et al., 2010; Murakami et al., 2022). As a consequence, the surface of the Earth crusted to progressively greater depths unless covered by overlying continental mass (Van Avendonk et al., 2016). The steady decline in amplitude of extinction events over the Phanerozoic Eon can now be explained by the observed decline in the concentration of CO_2, consistent with and required by the hypothesis that ocean acidification mediated by atmospheric CO_2 concentration was the most immediate cause of most past extinction events.

4.5. Temperature (Climate) Change and Mass Extinction Cycles

Numerous authors have proposed that extinction of biodiversity was caused by global climate change, and particularly by episodes of rapid global warming (e.g., Beerling & Berner, 2002; Clapham & Renne, 2019; Condamine et al., 2021; Gómez & Goy, 2011; Joachimski et al., 2012; McElwain et al., 1999, 2005; Petersen et al., 2016; Punekar et al., 2014; Song et al., 2021; Y. Sun et al., 2012; D. Sun et al., 2016; Vinós, 2022; Wilf et al., 2003). Climate (temperature) change is also the proposed kill mechanism of the P-T extinction ~252 Mya, based on stratigraphic evidence of a transition from low-energy meandering surface streams to high-energy braided streams in Northern China (Zhu et al., 2019) and worldwide (Benton & Newell, 2014; Ward et al., 2000). The most recent IPCC Assessment Report (AR6) asserts "with very high confidence" that "Extinction risk increases disproportionately from global warming of 1.5–3°C…" (IPCC, 2022, p. 56).

Extinction of biodiversity has also been attributed to climate change by Song et al. (2021), who report a strong positive correlation ($r = 0.76$) between biodiversity indices and temperature proxies, compared with the negligible correlation reported here ($r = 0.03$). Our contrasting findings may result from differences in data sources, sample resolution, data selection procedures and protocols, and related methodologies. In particular, their study developed a new Phanerozoic temperature proxy database that shows major differences from the dataset used here (Song et al., 2021, their Figure 1), including absence of the global temperature decline of 8–9°C over the Phanerozoic Eon, and absence of the ~130-Myr periodicity of Phanerozoic temperature that characterizes the temperature-proxy dataset of Prokoph et al. (2008) used widely and in the present study (see Figure 3 in W. J. Davis, 2017).

The present findings show that long-term (Myr) global temperature change, or climate, is not correlated discernibly with biodiversity loss during mass extinctions (Figure 17). The absence of correlation demonstrates the absence of causality. This study therefore excludes long-term temperature (climate) change as a possible cause of past mass extinctions. As summarized above, numerous studies instead support accelerated volcanic activity as the cause of increased atmospheric CO_2 concentration and consequent ocean acidification and anoxia, and mass extinction as the effect (Algeo et al., 2011; Benton & Twitchett, 2003; Bond & Grasby, 2017b; Burgess et al., 2017; Fox et al., 2022; Wignall & Twitchett, 1996; Wu et al., 2021). In this case the often-demonstrated linkage of past climate change with mass extinctions reflects correlation, not causation.

The finding here that long term temperature change was not the proximal cause of mass extinctions does not exclude shorter-term hyperthermals (e.g., Benton, 2018), which could not be detected at the Myr resolution of data used in this study. LIPs comprised molten magma seas or basalt floods (traps) covering up to a million square kilometers of the Earth's surface (Coffin & Eldholm, 1994). LIPs created lethal 35–40°C temperature spikes that eradicated life across broad marine and terrestrial areas and transiently heated and humidified the global atmosphere, altering regional and global rainfall. These accelerated volcanic events could also explain warming

of the Earth over millions of years as atmospheric CO_2 concentration declined (Figure 11). These same events are also plausible causes of the observed fluvial transitioning recorded in Northern China (Zhu et al., 2019) and globally (Benton & Newell, 2014; Ward et al., 2000). The resulting high-energy climate presumably contributed to biodiversity loss locally and regionally, without however displacing atmospheric CO_2 and consequent ocean acidification as the primary proximal cause of natural global mass extinctions.

Voluminous, converging evidence therefore supports the hypothesis that mass extinctions are explained primarily by the chemical and biological effects of CO_2 on ocean water and marine organisms operating through acidification and consequent reduction of primary production and anoxia, and not by the physical effects of the CO_2 molecule imparted by its greenhouse properties, that is, RF of temperature, as discussed next.

4.6. Radiative Forcing by Atmospheric Carbon Dioxide

Numerous previous authors have suggested a link between the concentration of atmospheric CO_2 and the loss of biodiversity during individual extinction events, as summarized above. The intermediary mechanism commonly proposed is the postulated increase in global temperature that is widely believed to result from increased atmospheric CO_2 concentration (but see W. J. Davis, 2017; W. J. Davis & Davis, 2020). A more direct measure of the global warming effect of trace gases such as CO_2 is RF computed at the top of the troposphere. If long-term global warming was the cause of past extinctions, then long-term temperature and marginal RF by atmospheric CO_2 should both be correlated positively with biodiversity loss.

As shown here, however, biodiversity loss is not correlated discernibly with marginal RF by atmospheric CO_2 ($r = -0.001$). Absence of correlation implies absence of causality, that is, changes in RF by atmospheric CO_2 did not cause past collapses in biodiversity and are not a plausible kill mechanism of mass extinctions. This finding reinforces and confirms the inference that long-term global warming is at most a correlate, and not a primary cause, of mass extinctions.

4.7. Additional Possible Kill Mechanisms of Mass Extinctions

While elevated atmospheric CO_2 and consequent ocean acidification and anoxia are the most likely immediate cause of most past mass extinctions, several associated forces presumably contributed. As noted above, the same LIPs that degas CO_2 to the atmosphere and acidify the ocean also create regional hyperthermic heat islands that exterminate life in the impacted region and induce short-term regional and global warming spikes. Accelerated volcanic activity that vents CO_2 also releases toxic gases (e.g., nitrous oxide, sulfur dioxide, hydrogen sulfide; Grice et al., 2005) that cause acid rains that in turn strip forests and soils and acidify the ocean to cause both anoxia and euxinia. Volcanism also releases toxic metals that can interfere with biological processes (e.g., Bond & Wignall, 2010; Font et al., 2016; Grasby et al., 2015, 2016; Percival et al., 2015; Sanei et al., 2012; Sial et al., 2013, 2014; Thibodeau et al., 2016; Vogt, 1972). These additional mechanisms all probably contributed in some measure to biodiversity loss during at least some past mass extinctions.

Reversals in the Earth's magnetic field have also been proposed as a possible cause of mass extinctions based on the apparent congruence of their spectral power periodicities (e.g., Creer & Pal, 1989; Raup, 1985). Other investigators, however, considered this congruence a methodological artifact (T. Lutz & Watson, 1988; see Puetz & Condie, 2022, for a review). Moreover, several mass extinctions occurred during superchrons—lengthy (tens of Myr) periods of constant geomagnetic field strength (Driscoll & Evans, 2016). Geomagnetic field reversals are therefore not necessary for the occurrence of mass extinctions, eliminating one of the two prerequisites for a causal relationship (necessity; see the discussion of causality criteria in the Discussion section of W. J. Davis & Davis, 2020). Changes in geomagnetic strength and consequent irradiation of Earth's surface by solar winds may also not be sufficient to cause widespread species radiation or extinction (Lingam, 2019; but see Channell & Vigliotti, 2019; Erdmann et al., 2021), potentially eliminating the second prerequisite for a causal relationship (sufficiency).

Geomagnetic reversals are more frequent during periods of diminished magma flow (Sheridan, 1997) and conversely (Olson & Amit, 2015), establishing a potential linkage of extinction events with mantle plumes and trap volcanic activity (LIPs; Radhakrishna et al., 2020). More recent studies also reconfirm spectral power peaks of geomagnetic reversals in the 16–40 Myr range (Melott et al., 2018). The present state of evidence therefore suggests that fluctuations in Earth's geomagnetic field are periodic at frequencies that at least overlap with those

of mass extinctions, implying that geomagnetic reversals may at least be correlated with geological forces that are causal to mass extinctions (Figure 3 in Barash, 2019; but see T. M. Lutz, 1985; T. Lutz & Watson, 1988). Direct causality has not been demonstrated, however, and it seems more likely that geomagnetic reversals and mass extinctions are influenced by a common third force, namely changes in mantle circulation patterns that emplace LIPs.

Similarly, combustion of forests (Mays & Mcloughin, 2022) and subterranean fossil fuel stores (Kaiho et al., 2021) triggered by bolide impacts and LIPs added GTs of CO_2 to the atmosphere to contribute to ocean acidification. Sea level reduction would reduce the most productive marine environments, continental shelf waters, as originally recognized by Newell (1952). Changes in sea level are correlated with geologic events associated with mass extinctions (J. Tennant et al., 2016, J. P. Tennant et al., 2016) and have been linked to mass extinctions (Sandberg et al., 2002). It is not clear, however, how reduced sea level could alone explain the simultaneous extinction of terrestrial genera that accompanied past collapses in marine biodiversity. Increased atmospheric CO_2 and consequent ocean acidification/anoxia are therefore the likely primary kill mechanism of mass extinctions, but a wave of secondary lethal effects is correlated and likely contributory, some of which operate through their effects on atmospheric CO_2 concentration (Fox et al., 2022).

4.8. Extraterrestrial Causes of Past Mass Extinctions

Theories of mass extinctions induced by extraterrestrial objects have been considered for more than 250 years (D'Hondt, 1998). In the modern era, Urey (1973) reinvigorated the hypothesis that comet and/or asteroid (bolide) showers are the ultimate cause of past extinction events. This hypothesis received empirical support from the discovery that the K-Pg extinction of the dinosaurs was associated with a large bolide impact ∼66 Mya (L. W. Alvarez et al., 1980) and, potentially, by bolide showers that extended over millions of years (L. Alvarez et al., 1984). Hundreds of authors have since reported common periodicities in diverse geological cycles that are approximately congruent with the cycles observed in impact crater age (e.g., L. Alvarez & Muller, 1984; Bailer-Jones, 2009; Baker & Flood, 2015; Boulila et al., 2018; Boulila, 2019; Chang & Moon, 2005; Creer & Pal, 1989; W. J. Davis, 2017; Hut et al., 1987; Isley & Abbot, 2002; Melott et al., 2018; Müller & Dutkiewicz, 2018; Prokoph et al., 2004; Prokoph et al., 2013; Rampino & Caldeira, 2020; Rampino & Stothers, 1984a, 1984b; Rampino et al., 2019; Rampino, 2015; but see Jetsu, 2011). A meta-review of 58 studies of impact crater age and 35 studies of extinction events shows that approximately two-thirds support statistically-significant cycling on a period of 26–29 Myr (Rampino & Prokoph, 2020). Another meta-review of 89 major geological events during the last 260 Myr supports consistent and statistically-significant Fourier spectral power peaks at ∼27.5 and 9–10 Myr (Rampino et al., 2021) across distinct geophysical and astrophysical cycles.

There is now overwhelming evidence that eight of the geophysical "Grand Cycles" (Boulila, 2019) are coupled with each other and oscillate at one or more of the three periodicities that characterize the age of impact craters on Earth, ∼10, 26 and 63 Myr. These cycles include volcanism (Abbott & Isley, 2002; Boulila, 2019; Clapham & Renne, 2019; Cogné & Humler, 2006; Isley & Abbot, 2002; Prokoph et al., 2013; Rampino et al., 2019), seafloor spreading (Baker & Flood, 2015; Cogné & Humler, 2006; Prokoph et al., 2004; Rich et al., 1986), plate tectonics (Abbott & Isley, 2002; Isley & Abbot, 2002; Kaiho & Saito, 1994; Prokoph et al., 2013), geomagnetic reversals (Creer & Pal, 1989; Raup, 1985), sea level (Baker & Flood, 2015; Boulila et al., 2018; House, 1985; Rampino & Caldeira, 2020), ocean acidity (Hinojosa et al., 2012; Rae et al., 2021), and mass extinction cycles (L. W. Alvarez et al., 1980; Baker & Flood, 2015; Bambach, 2006; Boulila, 2019; Boulila et al., 2018; Lieberman & Melott, 2012; Melott & Bambach, 2014; Prokoph et al., 2004; Rampino et al., 2019; Raup & Sepkoski, 1984; Rohde & Muller, 2005). The present study, together with previous research, adds an eighth Grand Cycle that oscillates at all three of the major periodicities of impact crater age (∼10, 26 and 63 Myr), namely the global carbon cycle as reflected by the concentration of CO_2 in Earth's atmosphere (W. J. Davis, 2017; Müller & Dutkiewicz, 2018; Rae et al., 2021).

The most robust correspondence between impact crater age and terrestrial geological periodicities is the 26 Myr cycle, which is also the most prominent rhythm in the atmospheric CO_2 paleo-record (Figure 6). The 26-Myr cycle is nearly identical in period to the half-period of oscillation of the Solar System during its back-and-forth journey across the galactic mid-plane (Rampino, 2001, 2015; Rampino & Caldeira, 2020). During such periodic crossovers, gravitational forces from dense matter concentrated at the galactic plane and/or nearby stars (Kramer & Rowan, 2022; Rampino, 2015; Rampino & Stothers, 1984a, 1984b) are postulated to create gravity waves that

perturb the Solar System's Oort comet cloud, composed largely of icy planetesimals, to generate bolide showers that impact Earth to induce tectonic activity leading to mass extinctions (Rampino, 2015).

Plausible astrophysical mechanisms therefore causally connect periodic bolide showers to geological cycles and mass extinctions, potentially explaining the prominent 26-Myr periodicity that characterizes all. The early studies of extraterrestrial causes of mass extinctions prompted dozens of subsequent investigations, which have provided a wealth of observational data in support of this hypothesis (e.g., Chang & Moon, 2005; Rampino & Prokoph, 2020). The continuing vigorous debate of the hypothesis (e.g., Bailer-Jones, 2011; Beauchamp & Grasby, 2012; Bond & Grasby, 2017b; Erlykin et al., 2017; Meier & Holm-Alwmark, 2017; Müller & Dutkiewicz, 2018) suggests that decisive evidence is lacking or at least limited. Others have noted that "Only the Chicxulub impact at the K/T [K-Pg] boundary 66.05 Mya has been linked to a mass extinction event…" (Schmieder & King, 2020, p. 119). The role of bolide impacts in past mass extinctions may be clarified by better dating of impact craters (Jetsu, 2011; Schmieder & King, 2020) on the Earth and Moon.

It remains theoretically possible that the congruent rhythms of the Grand Cycles including extraterrestrial bolide bombardment arise independently (Puetz & Condie, 2022). The probability of such coincidence, however, is infinitesimal. If only by exclusion, the preponderance of evidence suggests that the Grand Cycles, including atmospheric CO_2 fluctuations, are part of a causal chain initiated by galactic-scale forces. Shared harmonic periodicities between astrophysical, geophysical and biological cycles are otherwise difficult to explain. Such harmonic convergences suggest strongly, if circumstantially, a causal connection between collisions with extra-terrestrial objects and mass extinctions on Earth.

4.9. A Unified General Theory of Mass Extinction

Numerous authors have observed that the complete cause-and-effect framework of extinction cycles remains unclear (e.g., Larina et al., 2021). Evidence marshalled here and from the hundreds of previous studies on mass extinctions enables a plausible reconstruction of the causal chain from the initiation of a mass extinction cycle to the end of its recovery and the start of the next cycle. In this presumptive causal sequence, each extinction cycle is initiated when Earth passes through the galactic midplane every 26 Myr. During this passage, bolides from the Oort comet cloud are driven into the Earth's atmosphere by gravity waves from dense ordinary or dark matter concentrated at the galactic plane (Kramer & Rowan, 2022) to impact Earth's surface.

The mechanical and thermal energy associated with bolide impacts triggers or entrains pulsed plate tectonic movements, inducing mantle plume upwelling and associated surface disruptions that enhance global volcanic activity and release CO_2 to the atmosphere (Abbott & Isley, 2002; Hut et al., 1987; O'Neill et al., 2017; Sheridan, 1987a, 1987b, 1997; Renne et al., 2015; but see Ivanov & Melosh, 2003). Bolide bombardment of Earth's surface induces or entrains tectonic activity that generates or enhances volcanic activity in the form of LIPs (Abbott & Isley, 2002; Renne et al., 2015) to release subterranean CO_2 into the atmosphere and ocean, which acidifies the ocean to initiate mass extinctions (Black & Gibson, 2019; Fox et al., 2022; Wignall, 2015).

This initial chain of events accounts for the linkage between impact crater age, the terrestrial carbon cycle, and the 26-Myr atmospheric CO_2 cycle (W. J. Davis, 2017; Müller & Dutkiewicz, 2018). Independent evidence suggests that plate tectonic movements have affected atmospheric CO_2 levels (e.g., Van Der Meer et al., 2014), inducing for the last 545 Myr the 26-Myr periodicity of geological events (Boulila, 2019; Müller & Dutkiewicz, 2018; Rampino & Caldeira, 2020; Rampino et al., 2021; Rich et al., 1986) that are coupled with and the primary cause of past mass extinctions.

These geological forces, combined with regional hyperthermals, the release CO_2 to the atmosphere from burning flora and fauna (Mays & Mcloughin, 2022), and the combustion of subterranean stores of fossil fuels (Kaiho et al., 2021), acidify the ocean, exterminate the major marine primary producers (phytoplankton), and induce marine anoxia. Ocean anoxia teleconnects rapidly to land through the atmosphere (Beauchamp & Grasby, 2012) to exterminate terrestrial biodiversity, including especially large, oxygen-intensive homeotherms. Aerosols and particulate matter ejected into the atmosphere block sunlight transiently, impede photosynthetic activity on land, and add variably to the loss of species across different extinction events.

A complete theory of mass extinction cycles must explain the recovery (origination of new genera and species) that follows every such event. The operation of ancient sinks for CO_2 is not as well understood as CO_2 sources, but recent evidence supports the hypothesis that the periodic drawdown of atmospheric CO_2 following each peak in genus loss is caused by the weathering of new basalt crust after each LIP emplacement (e.g., Johansson

et al., 2018; Schobben et al., 2019). The reduced concentration of CO_2 in the atmosphere re-alkalinizes the ocean to restore pre-extinction pH levels, enabling the re-emergence of phytoplankton and the resumption of primary production, which releases the grip of anoxia on both the marine and terrestrial biosphere. Following recovery, the extinction cycle repeats with the return passage of the Solar System through the galactic midplane on its regular 26-Myr schedule, modulated by unidentified forces that impose the observed 10- and 63-Myr periodicities.

Many investigators have contributed to this theoretical reconstruction of mass extinctions, starting with Newell (1952), Raup and Sepkoski (1984), and Alvarez and colleagues (op. cit.), and continuing with Rampino (2001) and colleagues (Rampino et al., 2006, 2019), among others. This theory was outlined in rudimentary form 25 years ago (Tiwari & Rao, 1998) and developed further particularly by Rampino et al. (2006). Numerous studies by hundreds of investigators have since confirmed its main features and filled gaps, as summarized here.

This unified general theory of mass extinctions rationalizes several previously-puzzling features of Earth's history over geologic time, starting with the observed decline in atmospheric CO_2 concentration over the past 540 Myr (W. J. Davis, 2017; Royer, 2014; Figure 6 of this paper). The net global cooling of 8–9°C over the same period (Veizer et al., 1999; Veizer & Prokoph, 2015; Figure 3 in W. J. Davis, 2017), which may be explained by the simultaneous cooling of the mantle by 50°C (Murakami et al., 2022; Van Avendonk et al., 2016), has thickened the Earth's crust to its current depth of 5–70 km (Van Avendonk et al., 2016). A thickened crust reduces average LIP area and volume induced by bolide impacts and therefore limits direct venting of CO_2 from the underlying mantle (Coffin & Eldholm, 1994) and restricts cryptic venting (Armstrong-McKay et al., 2014), causing the observed overall decline in the atmospheric concentration of CO_2.

A thickening crust also forms an increasingly-protective armor against bolide bombardment and consequently reduces the area and volume of LIPs and the consequent volume of CO_2 transferred from subterranean magma stores to the atmosphere in sequential extinction events, as observed in the fossil record. Increased crustal thickness is expected to cause progressively smaller LIPs in response to bolide bombardment over deep time, also as observed (Coffin & Eldholm, 1994). Progressively smaller LIPs over geologic time imply proportionately smaller releases of CO_2 from subterranean sources to the atmosphere, as observed here in sequential 26 Myr atmospheric CO_2 cycles (Figure 6), and progressively smaller mass extinction events, as observed (Figure 1).

The weakest evidentiary link this proposed causal chain underlying mass extinctions may be astrophysical. Recent refinement of the age of known impact craters (Schmieder & King, 2020) may help clarify some of their relationships with the geological Grand Cycles. Whatever the remaining weaknesses in this general theory, it represents the most useful unified framework for further research on the nature and causes of mass extinctions.

4.10. The "Sixth Mass Extinction"

Judging from the history of past mass extinctions, the next natural cycle of extinction will occur in approximately 8.5 Myr and will be smaller than the last one. Earth would thus appear exempt from natural mass extinctions on timescales relevant to human civilizations. Numerous investigators have proposed, however, that in addition to the five canonical mass extinctions, the Earth is currently entering a sixth, human-induced period of mass extinction (e.g., Barnosky et al., 2011; Ceballos et al., 2015, 2020; Leakey & Lewin, 1995; Munstermann et al., 2021; Palombo, 2021; Payne et al., 2016). Such projections of biodiversity collapse have focused on the loss of terrestrial habitat and various forms of ecosphere pollution, and largely neglected the possible impact of elevated CO_2 and ocean acidification on marine biodiversity. As suggested here and by previous authors, however, extinction of biodiversity has been associated in the past with the demise of marine phytoplankton and the consequent loss of up to half the oxygen in the atmosphere (Falkowski et al., 1998; Field et al., 1998). Should this recur, it could render Earth uninhabitable to "advanced" life forms, particularly large, oxygen-intensive homeothermic species such as humans.

The fossil record provides the only long-term empirical data available for estimating the risk of such a global extinction event. The concentration of CO_2 in today's atmosphere, ~421 ppmv, is associated in the most recent fossil record with a 6.39% genus loss, similar to the genus loss associated with the smallest natural mass extinction event of the past (6.40%; extinction cycle # 10, 132.5 Mya, Figure 4). It follows that a significant fraction of marine life has already been exterminated by CO_2 emitted to the atmosphere by human activities. The best and only long-term empirical evidence available, the fossil record, therefore supports the inference that a "Sixth Mass Extinction" is not simply possible, plausible, or probable, but rather is already well underway and accelerating.

The fraction of life on Earth that may be lost in this human-made extinction can be estimated from the current rate of increase in the atmospheric concentration of CO_2, ~2 ppmv per year, which is caused almost entirely by anthropogenic emissions of CO_2 (IPCC, 2021, 2022). Knowing the number of genera and species on Earth, the cost in lost biodiversity of this ongoing Sixth Extinction can be calculated in the most graphic of terms, the number of species that disappear each day.

Toward this end, it has been estimated that Earth harbors 100,000 genera and 8.7 million (±1.3 million) species (Mora et al., 2011). At an annual increase of 2 ppmv in atmospheric concentration of CO_2, current human activities will raise atmospheric CO_2 from 421 to 441 ppmv in the next decade, corresponding to an increase in the loss of biodiversity from 6.3915% to 6.7735% (computed using Equation 1). The difference, 0.382% percent genus loss (6.7735%–6.3915%), implies the loss of 382 genera per decade (100,000 genera × 0.00382). Unless anthropogenic emissions of CO_2 are curbed immediately, therefore, at least 38.2 genera will become extinct every year over the next decade, equivalent to 3.18 genera per month ([38.2 genera/]/12 months) or 0.106 genera per day.

Converting this loss of genera to the estimated loss of species, the average extant genus contains 87 species (8.7 million species/100,000 genera) (Mora et al., 2011). Assuming for simplicity that the number of species is distributed equally across genera (which it is not), the estimated species extinction rate attributable to anthropogenic CO_2 emissions is 9.22 species per day (0.106 genera per day × 87 species per genus). Assuming that species loss from terrestrial sources caused by habitat reduction, pollution, climate change, etc., are equivalent to the marine losses projected here, human activities may be exterminating as many as 18 species per day. This loss is expected to grow proportionately with the continued increase in anthropogenic CO_2 emissions.

Estimating extinction rates has been described as a field "swimming in uncertainty" (Pearce, 2015), with widely different projections from prominent experts ranging from a few to more than 150 species lost every day. The preliminary projections made here from broadly-accepted fossil data suggest that the actual extinction rate is somewhere between the extremes previously suggested, but nearer the lower end of those estimates. Further human-induced extinction of marine life can be arrested only by stabilizing CO_2 in the atmosphere at a sufficiently low concentration. Past extinctions occurred at atmospheric CO_2 concentrations ranging from 249 to 2,772 ppmv, and at the current mean concentration of ~421 ppmv, it appears inevitable that some damage to marine life has already occurred. This damage is estimated here from the fossil record (Equation 1) as a 6.39% loss of genera.

Even if all anthropogenic CO_2 emissions ceased today, therefore, a significant extinction-level loss of biodiversity from human activities seems already assured. The outstanding question is whether a catastrophic, human-induced collapse of global biodiversity can be averted over the next century. The answer depends on the success of the transition to a carbon-neutral economy.

4.11. The Transition to a Carbon-Neutral Economy

Emplacement of a carbon-neutral economy, defined by zero net emissions of CO_2 from human activities, is the only way to slow and eventually stop the ongoing Sixth Mass Extinction. A smooth transition to a carbon-neutral economy requires balancing the risk of economic dislocation if emission cuts are too fast against the risk of human-induced mass extinction if emission cuts are too slow. The marginal benefit curve (Figure 21) provides the most efficient policy guidance, supporting smaller annual percent emission reductions stretched over longer periods of time.

Toward this end, a 1% yr^{-1} CO_2 reduction would yield zero anthropogenic net emissions by the year 2122 and a peak atmospheric CO_2 concentration of 621 ppmv, from which Equation 1 projects a biodiversity loss of 8.32%. This biodiversity loss is comparable to the losses of the two most recent natural extinction events, 8.3% and 8.8%, and nearly the same as the mean of the smallest nine extinctions of the last 210 Myr, 8.3%. A 2% yr^{-1} reduction in anthropogenic CO_2 emissions would yield zero net emissions by the year 2072, a maximum atmospheric CO_2 concentration of 472 ppmv, and an associated 7.37% biodiversity loss—a percentage point higher than the 6.39% genus loss associated with today's atmospheric CO_2 concentration of ~421 ppmv, but a percentage point lower than the biodiversity loss associated with the two most recent mass extinctions. A 3% yr^{-1} reduction would achieve even lower biodiversity loss (Figure 20), and would enable carbon neutrality by the year 2056, but would incur proportionately greater economic loss and risk from the premature retirement of existing fossil fuel capital
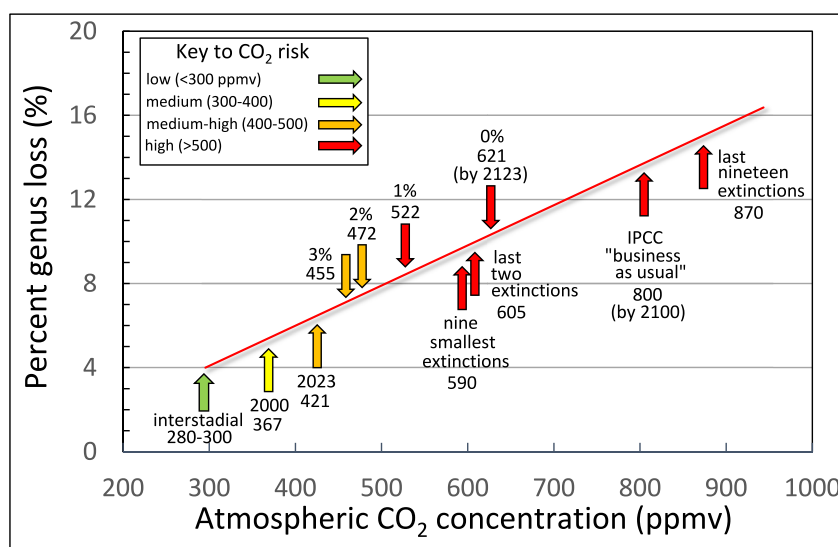
Figure 24. Extinction curve showing computed risks to biodiversity associated with atmospheric CO_2 reduction targets and milestones explored in this paper. Shown is the relationship between percent genus loss and atmospheric CO_2 concentration (red curve, best-fit linear trendline, method of least squares) based on the most recent fossil record (last 33 million year) (Figure 13a and Equation 1). The downward arrows above the extinction curve show the annual percent cuts required to achieve the stabilization of atmospheric carbon dioxide (CO_2) concentration at the levels shown in parts per million by volume (ppmv) by the dates shown in Figure 20. The upward arrows below the extinction curve mark CO_2 concentration milestones, starting with interstadial atmospheric CO_2 concentrations between recent Great Ice Ages (green arrow at lower left) and culminating in the mean atmospheric CO_2 concentration of the last 19 mass extinctions over the last 210 Myr (red arrow at upper right). This extinction curve shows that the loss of biodiversity associated with atmospheric CO_2 is already occurring, while losses of biodiversity comparable to past mass extinctions are projected for the near future. The units of all numbers except percentages and dates are ppmv. Abbreviations: CO_2, carbon dioxide; ppmv, parts per million by volume; IPCC, Intergovernmental Panel on Climate Change.

stock. An optimal rate of CO_2 emission reductions, that is, the reduction rate that achieves the most workable balance between economic well-being and biodiversity conservation, is 2% yr^{-1}.

The major results of this study are summarized and integrated on the extinction curve of Figure 24, which plots the regression of atmospheric CO_2 concentration on genus loss from the last 33 Myr of the fossil record (i.e., Figure 13a and Equation 1). Superimposed on the extinction curve in Figure 24 are CO_2 stabilization concentrations corresponding to different emission reduction scenarios (downward arrows above the red trendline) and natural and anthropogenic CO_2 milestones (upward arrows below the red trendline).

On the lower left of the extinction curve the interstadial concentration of CO_2 between GIAs is shown (green arrow), well below the concentration that causes significant loss of biodiversity. The concentration of atmospheric CO_2 in the year 2000, 367 ppmv, increased to 421 ppmv by the year 2023, a 54 ppmv increase in 23 years, implying the current 6.39% biodiversity loss. This risk to biodiversity is considered here as "medium-high" because it approaches the 6.4% loss that characterized the smallest mast extinction of the past (# 10 in Figure 4). On the upper right of the extinction curve in Figure 24, the concentration of CO_2 in Earth's atmosphere reaches 800 ppmv by the year 2100 (the IS92a scenario; IPCC, 1992). This projected concentration of atmospheric CO_2 approaches the mean of the last 19 mass extinctions over the past 210 Myr, computed here as 870 ppmv (range, 249–2,772 ppmv).

The effects of different emission reduction scenarios explored here are shown by downward arrows above the red extinction curve (Figure 24). These mark the CO_2 stabilization concentrations, that is, the maximum atmospheric CO_2 concentrations reached under the indicated emission reduction scenarios. Even the most practical emission reduction rates (2%–3% yr^{-1}) are associated with medium-high risk to biodiversity. The 1% yr^{-1} CO_2 reduction scenario creates a high risk to biodiversity in that it exceeds the mean CO_2 concentration and genus loss associated with the smallest nine extinctions on record over the last 534 Myr, 8.3%.

The energy policy that strikes the optimum balance between the economic costs of rapid carbon reduction and the ecological benefits of biodiversity preservation is a 2% yr^{-1} reduction in anthropogenic carbon emissions (Figure 21; third orange arrow from the left in Figure 24). This scenario, if implemented in the year 2023, would stabilize atmospheric CO_2 concentration by the year 2072 at 472 ppmv, associated in the fossil record with a cumulative biodiversity loss of 7.37% (Figures 20 and 24). The 2% yr^{-1} CO_2 reduction scenario still presents a significant risk to biodiversity, exceeding the minimum extinction-level of genus loss of 6.4% (event #10, 132.5 Mya; Figure 4). The 2% yr^{-1} emission reduction scenario may nonetheless be the most realistic target given the social, political and economic unknowns associated with the unprecedented transition to a carbon-neutral economy. Such a "cut your losses" strategy has the advantage of political plausibility, in that it is less ambitious than the consensus goal of the Paris Climate Agreement—a carbon-neutral economy by mid-century. Any slower rate of emission reductions would incur progressively greater risks to global biodiversity.

Thirteen years ago it was projected that using all available fossil-fuel energy infrastructure to the end of its lifetime and replacing it with the infrastructure of a carbon-neutral economy could stabilize atmospheric CO_2 concentration at 430 ppmv (S. J. Davis et al., 2010). The current concentration of CO_2 in the atmosphere is 421 ppmv and continues to increase at ∼2 ppmv yr^{-1}. At this rate of increase, the stabilization concentration of 430 ppmv projected by S. J. Davis et al. (2010) will be surpassed in less than 5 years, with no sign yet of carbon stabilization. This shortfall of reality from an informed expert projection made 13 years ago occurred despite the exponential increase in market penetration of renewable energy infrastructure over the same time period (Arndt et al., 2019; Jaeger, 2021; Lund, 2010).

The present study portrays a plausible path to carbon stabilization in a half-century at a peak atmospheric CO_2 concentration of 472 ppmv, assuming a 2% yr^{-1} reduction in net emissions that starts in 2023. Achieving this target and timetable will require, however, either accelerated market penetration of renewable energy resources (supply-side solutions), reduced consumption (demand-side solutions), or both.

Arresting the first global anthropogenic mass extinction therefore requires unprecedented reductions in anthropogenic CO_2 emission culminating in a carbon-neutral economy in less than a human lifetime. These realities imply limits to growth that may prove difficult to implement, imposing unprecedented challenges to systems of governance. A global policy framework for carbon reduction and biodiversity protection is available in the U.N. Law of the Sea Convention, the Framework Convention on Climate Change and the Convention on Biological Diversity. Within this international policy framework a new agreement on the conservation of biodiversity on the high seas is emerging (Barlow, 2021). Extant global policy instruments have not, however, reduced anthropogenic carbon emissions (Santos et al., 2022) nor slowed biodiversity loss, and a coordinated approach to ocean acidification has not yet emerged (VanderZwaag et al., 2021). These and other international and national legal frameworks and policy instruments are nonetheless positioned, in principle, to manifest a carbon-neutral world fast enough to stabilize atmospheric CO_2 at the threshold of extinction-level concentrations. It is therefore not too late to stop the first global mass extinction ever caused by humans.

Conflict of Interest

The author declares no conflicts of interest relevant to this study.

Data Availability Statement

Data used in this study are all from previously-published sources. Data on the marine fossil record of extinction are from J. J. Sepkoski (1986, 2002) and are tabulated in Table S1 in Supporting Information S1. Data on proxies of atmospheric carbon dioxide are from Royer (2014). Data on proxies of global temperature are from Prokoph et al. (2008). No previously-unpublished data were used in this study.

References

Abbott, D. H., & Isley, A. E. (2002). Extraterrestrial influences on mantle plume activity. *Earth and Planetary Science Letters*, *205*(1–2), 53–62. https://doi.org/10.1016/S0012-821X(02)01013-0

Algeo, T. J., Chen, Z. Q., Fraiser, M. L., & Twitchett, R. J. (2011). Terrestrial-marine teleconnections in the collapse and rebuilding of Early Triassic marine ecosystems. *Palaeogeography, Palaeoclimatology, Palaeoecology*, *308*(1–2), 1–11. https://doi.org/10.1016/j.palaeo.2011.01.011

Alvarez, L. W., Alvarez, W., Asaro, F., & Michel, H. V. (1980). Extraterrestrial cause for the Cretaceous-Tertiary extinction. *Science*, *208*(4448), 1095–1108. https://doi.org/10.1126/science.208.4448.1095

Alvarez, W., Kauffman, E. G., Michel, H. V., Alvarez, L. W., & Asaro, F. (1984). Impact theory of mass extinctions and the invertebrate fossil record. *Science*, *223*(4641), 1135–1141. https://doi.org/10.1126/science.223.4641.1135

Alvarez, W., & Muller, R. A. (1984). Evidence from crater age for periodic impacts on the Earth. *Nature*, *308*(5961), 718–720. https://doi.org/10.1038/308718a0

Alvarez-Fernandez, S., Bach, L. T., Taucher, J., Riebesell, U., Sommer, U., Aberle, N., et al. (2018). Plankton responses to ocean acidification: The role of nutrient limitation. *Progress in Oceanography*, *165*, 11–18. https://doi.org/10.1016/j.pocean.2018.04.006

Archibald, J. D., & Clemens, W. A. (1982). Late Cretaceous extinctions: The fossil evidence currently suggests that changes across the Cretaceous-Tertiary boundary were the result of gradual processes and not of a single event. *American Scientist*, *70*, 377–385. Retrieved from https://www.jstor.org/stable/27851545

Armstrong-McKay, D. I., Tyrrell, T., Wilson, P. A., & Foster, G. L. (2014). Estimating the impact of the cryptic degassing of Large Igneous Provinces: A mid-Miocene case-study. *Earth and Planetary Science Letters*, *403*, 254–262. https://doi.org/10.1016/j.epsl.2014.06.040

Arndt, C., Arent, D., Hartley, F., Merven, B., & Mondal, A. H. (2019). Faster than you think: Renewable energy and developing countries. *Annual Review of Resource Economics*, *11*(1), 149–168. https://doi.org/10.1146/annurev-resource-100518-093759

Bailer-Jones, C. A. L. (2009). The evidence for and against astronomical impacts on climate change and mass extinctions: A review. *International Journal of Astrobiology*, *8*(3), 213–239. https://doi.org/10.1017/S147355040999005X

Bailer-Jones, C. A. L. (2011). Evidence for variation—But no periodicity—In the terrestrial impact cratering rate. *EPSC Abstracts*, *6*. EPSC-DPS2011-153, 2011 EPSC-DPS Joint Meeting 2011. Retrieved from http://meetings.copernicus.org/epsc-dps2011

Baker, R. G. V., & Flood, P. G. (2015). The Sun-Earth connect 3: Lessons from the periodicities of deep time influencing sea-level change and marine extinctions in the geological record. *SpringerPlus*, *4*(1), 285. https://doi.org/10.1186/s40064-015-0942-6

Bambach, R. K. (2006). Phanerozoic biodiversity mass extinctions. *Annual Review of Earth and Planetary Sciences*, *34*(1), 127–155. https://doi.org/10.1146/annurev.earth.33.092203.122654

Bambach, R. K., Knoll, A. H., & Wang, S. (2004). Origination, extinction, and mass depletions of marine diversity. *Paleobiology*, *30*(4), 522–542. https://doi.org/10.1666/0094-8373(2004)030<0522LOEAMDO>2.0.CO;2

Barash, M. S. (2019). Changes in the geomagnetic field and the evolution of marine biota. *Oceanology*, *59*(2), 235–241. https://doi.org/10.1134/S0001437019020024

Barlow, E. (2021). Unprecedented marine biodiversity shifts necessitate innovation: The case for dynamic ocean management in the UN High-Seas Conservation Agreement. *Hastings Environmental Law Journal*, *27*, 121–143. Retrieved from https://repository.uchastings.edu/hastings_environmental_law_journal/vol27/iss2/5

Barnosky, A. D., Matzke, N., Tomiya, S., Wogan, G. O., Swartz, B., Quental, T. B., et al. (2011). Has the Earth's sixth mass extinction already arrived? *Nature*, *471*(7336), 51–57. https://doi.org/10.1038/nature09678

Baumert, H. Z., & Petzoldt, T. (2008). The role of temperature, cellular quota and nutrient concentrations for photosynthesis, growth and light-dark acclimation in phytoplankton. *Limnologica*, *38*(3–4), 313–326. https://doi.org/10.1016/j.limno.2008.06.002

Beauchamp, B., & Grasby, S. E. (2012). Permian lysocline shoaling and ocean acidification along NW Pangea led to carbonate eradication and chert expansion. *Palaeogeography, Palaeoclimatology, Palaeoecology*, *352*, 73–90. https://doi.org/10.1016/j.palaeo.2012.06.014

Beerling, D. J., & Berner, R. A. (2002). Biogeochemical constraints on the Triassic Jurassic boundary carbon cycle event. *Global Biogeochemical Cycles*, *16*(3), 10-1–10.13. https://doi.org/10.1029/2002GB001637

Benton, M. J. (2018). Hyperthermal-driven mass extinctions: Killing models during the Permian-Triassic mass extinction. *Philosophical Transactions of the Royal Society A*, *376*(2130), 20170076. https://doi.org/10.1098/rsta.2017.0076

Benton, M. J., & Newell, A. J. (2014). Impacts of global warming on Permo-Triassic terrestrial ecosystems. *Gondwana Research*, *25*(4), 1308–1337. https://doi.org/10.1016/j.gr.2012.12.010

Benton, M. J., & Twitchett, R. J. (2003). How to kill (almost) all life: The end-Permian extinction event. *Trends in Ecology and Evolution*, *18*(7), 358–365. https://doi.org/10.1016/S0169-5347(03)00093-4

Black, B. A., & Gibson, S. A. (2019). Deep carbon and the life cycle of large igneous provinces. *Elements*, *15*(5), 219–324. https://doi.org/10.2138/gselements.15.5.319

Bond, D., Wignall, P. B., & Racki, G. (2004). Extent and duration of marine anoxia during the Frasnian-Famennian (Late Devonian) mass extinction in Poland, Germany, Austria and France. *Geological Magazine*, *141*(2), 173–193. https://doi.org/10.1017/S0016756804008866

Bond, D. P. G. & Grasby, S. E. (Eds.). (2017a). Mass extinction causality: Records of anoxia, acidification, and global warming during Earth's greatest crises. *Palaeogeography, Palaeoclimatology, Palaeoecology*, *478*, 1–148. https://doi.org/10.1016/j.palaeo.2016.11.005

Bond, D. P. G., & Grasby, S. E. (2017b). On the causes of mass extinctions. *Palaeogeography, Palaeoclimatology, Palaeoecology*, *478*, 3–29. https://doi.org/10.1016/j.palaeo.2016.11.005

Bond, D. P. G., & Wignall, P. B. (2010). Pyrite framboid study of marine Permian−Triassic boundary sections: A complex anoxic event and its relationship to contemporaneous mass extinction. *Geological Society of America Bulletin*, *122*(7–8), 1265–1279. https://doi.org/10.1130/B30042.1

Bond, D. P. G., & Wignall, P. B. (2014). Large igneous provinces and mass extinctions: An update. In G. Keller & A. C. Kerr (Eds.), *Volcanism, impacts, and mass extinctions: Causes and effects, Geological Society of America special paper* (Vol. 505). https://doi.org/10.1130/2014.2505(02)

Boulila, S. (2019). Coupling between grand cycles and events in Earth's climate during the past 115 million years. *Nature, Science Reports*, *9*(1), 327. https://doi.org/10.1038/s41598-018-36509-7

Boulila, S., Laskar, J., Haq, B. U., Galbrun, B., & Hara, N. (2018). Phanerozoic sea-level sedimentary records and their potential drivers. *Global and Planetary Change*, *165*, 128–136. https://doi.org/10.1016/j.gloplacha.2018.03.004

Brenchley, P. J., Marshall, J. D., Carden, G. A. F., Robertson, D. B. R., Long, D. G. F., Meidla, T., et al. (1994). Bathymetric and isotopic evidence for a short-lived Late Ordovician glaciation in a greenhouse period. *Geology*, *22*(4), 295–298. https://doi.org/10.1130/0091-7613(1994)022<0295:BAIEFA>2.3.CO;2

Brenchley, P. J., Marshall, J. D., & Underwood, C. J. (2001). Do all mass extinctions represent an ecological crisis? Evidence from the Late Ordovician. *Geological Journal*, *36*(3–4), 329–340. https://doi.org/10.1002/gj.880

Brewer, P. G. A. (2013). A short history of ocean acidification science in the 20th century: A chemist's view. *Biogeosciences*, *10*(11), 7411–7422. https://doi.org/10.5194/bg-10-7411-2013

Brocks, J., Jarrett, A., Sirantoine, E., Hallmann, C., Hoshino, Y., & Liyanage, T. (2017). The rise of algae in Cryogenian oceans and the emergence of animals. *Nature*, *548*(7669), 578–581. https://doi.org/10.1038/nature23457

Buggisch, W. (1991). The global Frasnian-Famennian 'Kellwasser Event'. *Geologische Rundschau*, *80*(1), 49–72. https://doi.org/10.1007/BF01828767

Burgess, S. D., Muirhead, J. D., & Bowring, S. A. (2017). Initial pulse of Siberian Traps sills as the trigger of the end-Permian mass extinction. *Nature Communications*, *8*(1), 164. https://doi.org/10.1038/s41467-017-00083-9

Capriolo, M., Mills, B. J. W., Newton, R. J., Corso, J.-D., Dunhill, A. M., Wignall, P. B., & Marzoli, A. (2022). Anthropogenic-scale CO_2 degassing from the Central Atlantic Magmatic Province as a driver of the end-Triassic mass extinction. *Global and Planetary Change*, *209*, 103731. https://doi.org/10.1016/j.gloplacha.2021.103731

Ceballos, G., Ehrlich, P. R., Barnosky, A. D., García, A., Pringle, R. M., & Palmer, T. M. (2015). Accelerated modern human–induced species losses: Entering the sixth mass extinction. *Science Advances*, *1*(5), e1400253. https://doi.org/10.1126/sciadv.1400253

Ceballos, G., Ehrlich, P. R., & Raven, P. H. (2020). Vertebrates on the brink as indicators of biological annihilation and the sixth mass extinction. *Proceedings of the National Academy of Sciences USA*, *117*(24), 13596–13602. https://doi.org/10.1073/pnas.1922686117

Chang, H.-Y., & Moon, H.-K. (2005). Time-series analysis of terrestrial impact crater records. *Publications of the Astronomical Society of Japan*, *57*(3), 487–495. https://doi.org/10.1093/pasj/57.3.487

Channell, J. E. T., & Vigliotti, L. (2019). The role of geomagnetic field intensity in Late Quaternary evolution of humans and large mammals. *Reviews of Geophysics*, *57*(3), 709–738. https://doi.org/10.1029/2018RG000629

Chen, Q., Liu, H., Johnson, T., Hartnady, M., Kirkland, C., Lu, Y., & Sun, W.-D. (2022). Intraplate continental basalts over the past billion years track cooling of the mantle and the onset of modern plate tectonics. *Earth and Planetary Science Letters*, *597*, 117804. https://doi.org/10.1016/j.epsl.2022.117804

Clapham, M. E., & Payne, J. L. (2011). Acidification, anoxia, and extinction: A multiple logistic regression analysis of extinction selectivity during the Middle and Late Permian. *Geology*, *39*(11), 1059–1062. https://doi.org/10.1130/G32230.1

Clapham, M. E., & Renne, P. R. (2019). Flood basalts and mass extinctions. *Annual Review of Earth and Planetary Sciences*, *47*(1), 275–303. https://doi.org/10.1146/annurev-earth-053018-060136

Clarkson, M. O., Kasemann, S. A., Wood, R. A., Lenton, T. M., Daines, S. J., Richoz, S., et al. (2015). Ocean acidification and the Permo-Triassic mass extinction. *Science*, *348*(6231), 229–232. https://doi.org/10.1126/science.aaa0193

Coffin, M. F., & Eldholm, O. (1994). Large igneous provinces: Crustal structure, dimensions, and external consequences. *Reviews of Geophysics*, *32*, 1–36. https://doi.org/10.1029/93RG02508

Cogné, J.-P., & Humler, E. (2006). Trends and rhythms in global seafloor generation rate. *Geochemistry, Geophysics, Geosystems*, *7*(3), Q03011. https://doi.org/10.1029/2005GC001148

Condamine, F. L., Guinot, G., Benton, M. J., & Currie, P. J. (2021). Dinosaur biodiversity declined well before the asteroid impact, influenced by ecological and environmental pressures. *Nature Communications*, *12*(1), 3833. https://doi.org/10.1038/s41467-021-23754-0

Condie, K. C., Aster, R. C., & Van Hunen, J. (2016). A great thermal divergence in the mantle beginning 2.5 Ga: Geochemical constraints from greenstone basalts and komatiites. *Geoscience Frontiers*, *7*(4), 543–553. https://doi.org/10.1016/j.gsf.2016.01.006

Creer, K. M., & Pal, P. C. (1989). On the frequency of reversals of the geomagnetic dipole. In *Catastrophes and evolution: Astronomical foundations; Proceedings of the 1988 BAAS Mason meeting of the Royal Astronomical Society, Oxford, England, Sept. 6, 1988 (A90-44210 19-88)* (pp. 113–132). Cambridge University Press. Retrieved from http://pascal-francis.inist.fr/vibad/index.php?action=getRecordDetail&idt=19259871

Dal Corso, J., Song, H., Callegaro, S., Chu, D., Sun, Y., Hilton, J., et al. (2022). Environmental crises at the Permian–Triassic mass extinction. *Nature Reviews Earth and Environment*, *3*, 197–214. https://doi.org/10.1038/s43017-021-00259-4

Davis, S. J., Caldeira, K., & Matthews, H. D. (2010). Future CO_2 emissions and climate change from existing energy infrastructure. *Science*, *329*(5997), 1330–1333. https://doi.org/10.1126/science.1188566

Davis, W. J. (2017). The relationship between atmospheric carbon dioxide concentration and global temperature for the last 425 million years. *Climate*, *5*(4), 76. https://doi.org/10.3390/cli5040076

Davis, W. J., & Davis, W. B. (2020). Antarctic winds: Pacemaker of global warming, global cooling, and the collapse of civilizations. *Climate*, *8*(11), 130. https://doi.org/10.3390/cli8110130

Davis, W. J., Taylor, P. J., & Davis, W. B. (2018). The Antarctic Centennial Oscillation: A natural paleoclimate cycle in the Southern Hemisphere that influences global temperature. *Climate*, *6*(1), 3. https://doi.org/10.3390/cli6010003

Davis, W. J., Taylor, P. J., & Davis, W. B. (2019). The origin and propagation of the Antarctic Centennial Oscillation. *Climate*, *7*(9), 112. https://doi.org/10.3390/cli7090112

D'Hondt, S. (1998). Theories of terrestrial mass extinction by extraterrestrial objects. *Earth Sciences History*, *17*(2), 157–173. https://doi.org/10.17704/eshi.17.2.3g635053823v0h23

Donahue, K., Klaas, C., Dillingham, P. W., & Hoffmann, L. J. (2019). Combined effects of ocean acidification and increased light intensity on natural phytoplankton communities from two southern ocean water masses. *Journal of Plankton Research*, *41*(1), 30–45. https://doi.org/10.1093/plankt/fby048

Doney, S. C., Busch, D. S., Cooley, S. R., & Kroeker, K. J. (2020). The impacts of ocean acidification on marine ecosystems and reliant human communities. *Annual Review of Environment and Resources*, *45*(1), 83–112. https://doi.org/10.1146/annurev-environ-012320-083019

Doney, S. C., Fabry, V. J., Feely, R. A., & Kleypas, J. A. (2009). Ocean acidification: The other CO_2 problem. *Annual Review of Marine Sciences*, *1*, 169–192. https://doi.org/10.1146/annurev.marine.010908.163834

Driggers, R. G., Friedman, M. H., & Nicols, J. M. (2012). *An introduction to infrared and electro-optical systems* (2nd ed.). Artech House. ISBN 13:978-1-60807-100-5.

Driscoll, P. E., & Evans, D. A. (2016). Frequency of Proterozoic geomagnetic superchrons. *Earth and Planetary Science Letters*, *437*, 9–14. https://doi.org/10.1016/j.epsl.2015.12.035

Duarte, C. M., & Cebrian, J. (1996). The fate of marine autotrophic production. *Limnology and Oceanography*, *41*(8), 1758–1766. https://doi.org/10.4319/lo.1996.41.8.1758

Dutkiewicz, S., Morris, J. J., Follows, M. J., Scott, J., Levitan, O., Dyhrman, S. T., & Berman-Frank, I. (2015). Impact of ocean acidification on the structure of future phytoplankton communities. *Nature Climate Change*, *5*(11), 1002–1006. https://doi.org/10.1038/nclimate2722

Eberlein, T., Wohlrab, S., Rost, B., John, U., Bach, L. T., Riebesell, U., & Van der Waal, D. B. (2017). Effects of ocean acidification on primary production in a coastal North Sea phytoplankton community. *PLoS One*, *12*(3), e0172594. https://doi.org/10.1371/journal.pone.0172594

Erdmann, W., Kmita, H., Kosicki, J. Z., & Kaczmarek, Ł. (2021). How the geomagnetic field influences life on Earth – An integrated approach to geomagnetobiology. *Origin of Life and Evolution of Biospheres*, *51*(3), 231–257. https://doi.org/10.1007/s11084-021-09612-5

Erlykin, A. D., Harper, D. A. T., Sloan, T., & Wolfendale, A. W. (2017). Mass extinctions over the last 500 Myr: An astronomical cause? *Paleontology*, *60*(2), 159–167. https://doi.org/10.1111/pala.12283

IPCC. (1992). *Climate change 1992, supplement*. World Meteorological Organization. ISBN 0 521 43829 2.

IPCC. (2001). In J. T. Houghton (Ed.), *Climate change 2001: The scientific basis*. Cambridge University Press. ISBN # 0 521 80770 0.

IPCC. (2007). In S. Solomon (Ed.), *Climate change 2007: The physical science basis; Contribution of Working Group I to the fourth assessment report of the Intergovernmental Panel on Climate Change*. Cambridge University Press. ISBN 9780521705967.

IPCC. (2013). In T. F. Stocker (Ed.), *Climate change 2013: The physical science basis; Contribution of Working Group I to the fifth assessment report of the Intergovernmental Panel on Climate Change*. Cambridge University Press. ISBN 978-1-107-05799-9.

IPCC. (2021). In S. L. Connors, C. Péan, S. Berger, N. Caud, Y. Chen, et al. (Eds.), *Climate change 2021: The physical science basis. Contribution of Working Group I to the sixth assessment report of the Intergovernmental Panel on Climate Change*. Cambridge University Press. ISBN 978-92-9169-158-6.

IPCC. (2022). In H.-O. Pörtner, D. C. Roberts, M. Tignor, E. S. Poloczanska, K. Mintenbeck, et al. (Eds.), *Climate change 2022: Impacts, adaptation and vulnerability. Contribution of Working Group II to the sixth assessment report of the Intergovernmental Panel on Climate Change* (p. 3056). Cambridge University Press. https://doi.org/10.1017/9781009325844

Isley, A. E., & Abbot, D. H. (2002). Implications of the temporal distribution of high-Mg magmas for mantle plume volcanism through time. *Journal of Geology*, *110*(2), 141–158. https://doi.org/10.1086/338553

Isozaki, Y. (1997). Permo-Triassic boundary superanoxia and stratified superocean: Records from lost deep sea. *Science*, *276*(5310), 235–238. Retrieved from https://www.jstor.org/stable/2892752

Ivanov, B. A., & Melosh, H. J. (2003). Impacts do not initiate volcanic eruptions: Eruptions close to the crater. *Geology*, *31*(10), 869–872. https://doi.org/10.1130/G19669.1

Jaeger, J. (2021). *Explaining the exponential growth of renewable energy*. World Resources Institute. Retrieved from https://www.wri.org/insights/growth-renewable-energy-sector-explained

Jetsu, L. (2011). Some studies of terrestrial impact cratering rate. *Baltic Astronomy*, *20*(2), 289–296. https://doi.org/10.1515/astro-2017-0294

Jiang, L.-Q., Carter, B. R., Feely, R. A., Lauvset, S. K., & Olsen, A. (2019). Surface ocean pH and buffer capacity: Past, present and future. *Scientific Reports*, *9*(1), 18624. https://doi.org/10.1038/s41598-019-55039-4

Joachimski, M. M., Lai, X., Shen, S., Jiang, H., Luo, G., Chen, B., et al. (2012). Climate warming in the latest Permian and the Permian-Triassic mass extinction. *Geology*, *40*(3), 195–198. https://doi.org/10.1130/G32707.1

Johansson, L., Zahirovic, S., & Müller, R. D. (2018). The interplay between the eruption and weathering of Large Igneous Provinces and the deep-time carbon cycle. *Geophysical Research Letters*, *45*(11), 5380–5389. https://doi.org/10.1029/2017GL076691

Jurikova, H., Gutjahr, M., Wallmann, K., Flögel, S., Liebetrau, V., Posenato, R., et al. (2020). Permian–Triassic mass extinction pulses driven by major marine carbon cycle perturbations. *Nature Geoscience*, *13*(11), 745–750. https://doi.org/10.1038/s41561-020-00646-4

Kaiho, K., Aftabuzzaman, M., Jones, D. S., & Tian, L. (2021). Pulsed volcanic combustion events coincident with the end-Permian terrestrial disturbance and the following global crisis. *Geology*, *49*(3), 289–293. https://doi.org/10.1130/G48022.1

Kaiho, K., & Saito, S. (1994). Oceanic crust production and climate during the last 100 Ma. *Terra Nova*, *6*(4), 376–384. https://doi.org/10.1111/j.1365-3121.1994.tb00510.x

Keller, G., Mateo, P., Monkenbusch, J., Thibault, N., Punekar, J., Spangenberg, J. E., et al. (2020). Mercury linked to Deccan Traps volcanism, climate change and the end-Cretaceous mass extinction. *Global and Planetary Change*, *194*, 103312. https://doi.org/10.1016/j.gloplacha.2020.103312

Kidder, D. L., & Worsley, T. R. (2010). Phanerozoic Large Igneous Provinces (LIPs), HEATT (Haline Euxinic Acidic Thermal Transgression) episodes, and mass extinctions. *Palaeoecology*, *295*(1–2), 162–191. https://doi.org/10.1016/j.palaeo.2010.05.036

Kiessling, W., & Simpson, C. (2011). On the potential for ocean acidification to be a general cause of ancient reef crises. *Global Change Biology*, *17*(1), 56–67. https://doi.org/10.1111/j.1365-2486.2010.02204.x

Knoll, A. H. (1984). Patterns of extinction in the fossil record of vascular plants. In M. H. Nitecki (Ed.), *Extinctions* (pp. 21–68). Chicago Univ. Press. https://doi.org/10.1017/CB09780511607370.004

Kramer, E. D., & Rowan, M. (2022). Revisiting the dark matter-comet shower connection. *Physics of the Dark Universe*, *35*, 100960. https://doi.org/10.1016/j.dark.2022.100960

Kroeck, D. M., Mullins, G., Zacai, A., Monnet, C., & Servais, T. (2022). A review of Paleozoic phytoplankton biodiversity: Driver for major evolutionary events? *Earth-Science Reviews*, *232*, 104113. https://doi.org/10.1016/j.earscirev.2022.104113

Larina, E., Bottjer, D., Corsetti, F., Thibodeau, A., Berelson, W., West, A. J., & Yager, J. (2021). Ecosystem change and carbon cycle perturbation preceded the end-Triassic mass extinction. *Earth and Planetary Science Letters*, *576*, 117180. https://doi.org/10.1016/J.EPSL.2021.117180

Leakey, R. E., & Lewin, R. (1995). *The sixth extinction: Biodiversity and its survival* (p. 288). Phoenix Publishers. ISBN 978-0297817338.

Lieberman, B. S., & Melott, A. L. (2012). Whilst this planet has gone cycling on: What role for periodic astronomical phenomena in large-scale patterns in the history of life? In J. A. Talent (Ed.), *Earth and life, international year of planet Earth* (pp. 37–50). Springer Science and Business Media B.V. https://doi.org/10.1007/978-90-481-3428-1_3

Lingam, M. (2019). Revisiting the biological ramifications of variations in Earth's magnetic field. *Astrophysical Journal Letters*, *874*(2), L28. https://doi.org/10.3847/2041-8213/ab12eb

Lund, P. D. (2010). Fast market penetration of energy technologies in retrospect with application to clean energy futures. *Applied Energy*, *87*(11), 3575–3583. https://doi.org/10.1016/j.apenergy.2010.05.024

Lutz, T., & Watson, G. (1988). Effects of long-term variation on the frequency spectrum of the geomagnetic reversal record. *Nature*, *334*(6179), 240–242. https://doi.org/10.1038/334240a0

Lutz, T. M. (1985). The magnetic reversal record is not periodic. *Nature*, *317*(6036), 404–407. https://doi.org/10.1038/317404a0

Martindale, R. C., Berelson, W. M., Corsetti, F. A., Bottjer, D. J., & West, A. J. (2012). Constraining carbonate chemistry at a potential ocean acidification event (the Triassic Jurassic boundary) using the presence of corals and coral reefs in the fossil record. *Palaeogeography, Palaeoclimatology, Palaeoecology*, *350–352*, 114–123. https://doi.org/10.1016/j.palaeo.2012.06.020

Mays, C., & Mcloughin, S. (2022). End-Permian burnout: The role of Permian–Triassic wildfires in extinction, carbon cycling, and environmental change in eastern Gondwana. *PALAIOS*, *37*(6), 292–317. https://doi.org/10.2110/palo.2021.051

McElwain, J. C., Beerling, D. J., & Woodward, F. I. (1999). Fossil plants and global warming at the Triassic-Jurassic Boundary. *Science*, *285*(5432), 1386–1390. https://doi.org/10.1126/science.285.5432.1386

McElwain, J. C., Wade-Murphy, J., & Hesselbo, S. P. (2005). Changes in carbon dioxide during an oceanic anoxic event linked to intrusion into Gondwana coals. *Nature*, *435*(7041), 479–482. https://doi.org/10.1038/nature03618

Meier, M. M. M., & Holm-Alwmark, S. (2017). A tale of clusters: No resolvable periodicity in the terrestrial impact cratering record. *Monthly Notices of the Royal Astronomical Society*, *467*, 2545–2551. https://doi.org/10.1093/mnras/stx211

Mélançon, J., Levasseur, M., Lizotte, M., Scarratt, M., Tremblay, J.-E., Tortell, P., et al. (2016). Impact of ocean acidification on phytoplankton assemblage, growth, and DMS production following Fe-dust additions in the NE Pacific high-nutrient, low-chlorophyll waters. *Biogeosciences*, *13*(5), 1677–1692. https://doi.org/10.5194/bg-13-1677-2016

Melott, A. L., & Bambach, R. K. (2014). Analysis of periodicity of extinction using the 2012 geological timescale. *Paleobiology*, *40*(2), 177–196. https://doi.org/10.1666/13047

Melott, A. L., Pivarunas, A., Mert, J. G., & Lieberman, B. S. (2018). Does the planetary dynamo go cycling on? Re-examining the evidence for cycles in magnetic reversal rate. *International Journal of Astrobiology*, *17*(1), 44–50. https://doi.org/10.1017/S1473550417000040

Montenegro, A., Spence, P., Meissner, K. J., Eby, M., Melchin, M. J., & Johnston, S. T. (2011). Climate simulations of the Permian-Triassic boundary: Ocean acidification and the extinction event. *Paleoceanography*, *26*(3), PA3207. https://doi.org/10.1029/2010PA002058

Mora, C., Tittensor, D. P., Adl, S., Simpson, A. G. B., & Worm, B. (2011). How many species are there on Earth and in the ocean? *PLoS Biology*, *9*(8), e1001127. https://doi.org/10.1371/journal.pbio

Müller, R. D., & Dutkiewicz, A. (2018). Oceanic crustal carbon cycle drives 26-million year atmospheric carbon dioxide periodicities. *Scientific Advances*, *4*(2), eaaq0500. https://doi.org/10.1126/sciadv.aaq0500

Munstermann, M. J., Heim, N. A., McCauley, D. J., Payne, J. L., Upham, N. S., Wang, S. C., & Knope, M. L. (2021). A global ecological signal of extinction risk in terrestrial vertebrates. *Conservation Biology*, *36*(3), e13852. https://doi.org/10.1111/cobi.13852

Murakami, M., Goncharov, A. F., Miyajima, N., Yamazaki, D., & Holtgrewe, N. (2022). Radiative thermal conductivity of single-crystal bridgmanite at the core-mantle boundary with implications for thermal evolution of the Earth. *Earth and Planetary Science Letters*, *578*, 117329. https://doi.org/10.1016/j.epsl.2021.117329

NASA. NASA Earth Observatory. (2022). *Global temperatures*. Earth Observatory. Retrieved from https://earthobservatory.nasa.gov/world-of-change/decadaltemp.php

Newell, N. D. (1952). Periodicity in invertebrate evolution. *Journal of Paleontology*, *26*, 371–385. Retrieved from https://www.jstor.org/stable/1299949

Newell, N. D. (1962). Paleontological gaps and geochronology. *Journal of Paleontology*, *3*, 592–610. Retrieved from https://www.jstor.org/stable/1301092

Newell, N. D. (1963). Crises in the history of life. *Scientific American*, *76–92*(2), 76–93. Retrieved from https://www.jstor.org/stable/24936467

Newell, N. D. (1967). Revolutions in the history of life. In C. C. Albritton (Ed.), *Uniformity and simplicity*, *Geological Society of America special paper* (Vol. 89, pp. 63–91). https://doi.org/10.1130/SPE89-p63

NOAA. (2020). Retrieved from https://research.noaa.gov/article/ArtMID/587/ArticleID/2636/Rise-of-carbon-dioxide-unabated

NOAA. (2021). Retrieved from https://research.noaa.gov/article/ArtMID/587/ArticleID/2764/Coronavirus-response-barely-slows-rising-carbon-dioxide

Olson, P., & Amit, H. (2015). Mantle superplumes induce geomagnetic superchrons. *Frontiers in Earth Science*, *3*, 38. https://doi.org/10.3389/feart.2015.00038

O'Neill, C., Marchi, S., Zhang, S., & Bottke, W. (2017). Impact-driven subduction on the Hadean Earth. *Nature Geoscience*, *10*, 793–797. https://doi.org/10.1038/ngeo3029

Palombo, M. R. (2021). Thinking about the biodiversity loss in this changing world. *Geosciences*, *11*(9), 370. https://doi.org/10.3390/geosciences11090370

Payne, J. L., Bush, A. M., Heim, N. A., Knope, M. L., & McCauley, D. J. (2016). Ecological selectivity of the emerging mass extinction in the oceans. *Science*, *353*(6305), 1284–1286. https://doi.org/10.1126/science.aaf2416

Payne, J. L., Lehrmann, D. J., Follett, D., Seibel, M., Kump, L. R., Riccardi, A., et al. (2007). Erosional truncation of uppermost Permian shallow-marine carbonates and implications for Permian-Triassic boundary events. *Geological Society of America Bulletin*, *119*(7–8), 771–784. https://doi.org/10.1130/B26091.1

Pearce, F. (2015). Global extinction rates: Why do estimates vary so widely? Retrieved from https://e360.yale.edu/features/global_extinction_rates_why_do_estimates_vary_so_wildly

Peña, V., Harvey, B. P., Agostini, S., Porzio, L., Milazzo, M., Horta, P., et al. (2021). Major loss of coralline algal diversity in response to ocean acidification. *Global Change Biology*, *27*(19), 4785–4798. https://doi.org/10.1111/gcb.15757

Percival, L. M. E., Witt, M. L. I., Mather, T. A., Hermoso, M., Jenkyns, H. C., Hesselbo, S. P., et al. (2015). Globally enhanced mercury deposition during the end-Pliensbachian extinction and Toarcian OAE: A link to the Karoo-Ferrar Large Igneous Province. *Earth and Planetary Science Letters*, *428*, 267–280. https://doi.org/10.1016/j.epsl.2015.06.064

Petersen, S. V., Dutton, A., & Lohmann, K. C. (2016). End-Cretaceous extinction in Antarctica linked to Deccan volcanism and meteorite impact via climate change. *Nature Communications*, *7*(1), 12079. https://doi.org/10.1038/ncomms12079

Prokoph, A., Bilali, H. E., & Ernst, R. (2013). Periodicities in the emplacement of large igneous provinces through the Phanerozoic: Relations to ocean chemistry and marine biodiversity. *Geoscience Frontiers*, *4*(3), 263–276. https://doi.org/10.1016/j.gsf.2012.08.001

Prokoph, A., Rampino, M. R., & Bilali, H. E. (2004). Periodic components in the diversity of calcareous plankton and geological events over the past 230 M. *Paleoecology*, *207*(1–2), 105–125. https://doi.org/10.1016/j.palaeo.2004.02.004

Prokoph, A., Shields, G. A., & Veizer, J. (2008). Compilation and time-series analysis of a marine carbonate $\delta^{18}O$, $\delta^{13}C$, $^{87}Sr/^{86}Sr$ and $\delta^{34}S$ database through Earth history. *Earth-Science Reviews*, *87*(3–4), 113–133. https://doi.org/10.1016/j.earscirev.2007.12.003

Puetz, S. J., & Condie, K. C. (2022). A review of methods used to test periodicity of natural processes with a special focus on harmonic periodicities found in global UPb detrital zircon age distributions. *Earth-Science Reviews*, *224*, 103885. https://doi.org/10.1016/j.earscirev.2021.103885

Punekar, J., Mateo, P., & Keller, G. (2014). Effects of Deccan volcanism on paleoenvironment and planktic foraminifera: A global survey. In G. Keller & A. C. Kerr (Eds.), *Volcanism, impacts, and mass extinctions: Causes and effects*, *Geological Society of America special paper* (Vol. 505, pp. 91–116). https://doi.org/10.1130/2014.250(04)

Radhakrishna, T., Asanulla, R., Mohamed, A. R., Venkateshwarlu, M., & Soumya, G. S. (2020). Low geomagnetic field strength during End-Cretaceous Deccan volcanism and whole mantle convection. *Scientific Reports*, *10*(1), 10743. https://doi.org/10.1038/s41598-020-67245-6

Rae, J. W. B., Zhang, Y. G., Liu, X., Foster, G. L., Stoll, H. M., & Whiteford, R. D. M. (2021). Atmospheric CO_2 over the past 66 million years from marine archives. *Annual Review of Earth and Planetary Sciences*, *49*(1), 609–641. https://doi.org/10.1146/annurev-earth-802420-063026

Rahlff, J., Stolle, C., Giebel, H.-A., Ribas-Ribas, M., Damgaard, L. R., & Wurl, O. (2019). Oxygen profiles across the sea-surface microlayer—Effects of diffusion and biological activity. *Frontiers in Marine Science*, *6*, 11. https://doi.org/10.3389/fmars.2019.00011

Rampino, M. R. (2001). Galactic triggering of periodic comet showers and mass extinctions on Earth. In M. Y. Marov & H. Rickman (Eds.), *Collisional processes in the solar system* (p. 261). Springer. Astrophysics and Space Science Library. https://doi.org/10.1007/978-94-010-0712-2_6

Rampino, M. R. (2015). Disc dark matter in the galaxy and potential cycles of extraterrestrial impacts, mass extinctions and geological events. *Monthly Notices of the Royal Astronomical Society*, *448*(2), 1816–1819. https://doi.org/10.1093/mnras/stu2708

Rampino, M. R., & Caldeira, K. (2020). A 32-million year cycle detected in sea-level fluctuations over the last 545 M. *Geoscience Frontiers*, *11*(6), 2061–2065. https://doi.org/10.1016/j.gsf.2020.06.005

Rampino, M. R., Caldeira, K., & Prokoph, A. (2019). What causes mass extinctions? Large asteroid/comet impacts, flood-basalt volcanism, and ocean anoxia—Correlations and cycles. In C. Koeberl & D. M. Bice (Eds.), *250 million years of Earth history in Central Italy: Celebrating 25 years of the geological observatory of Coldigioco, Geological Society of America special paper* (Vol. 542, pp. 271–302). https://doi.org/10.1130/2019.2542(14)

Rampino, M. R., Caldeira, K., & Zhu, Y. (2021). A pulse of the Earth: A 27.5-Myr underlying cycle in coordinated geological events over the last 260 M. *Geoscience Frontiers*, *12*(6), 101245. https://doi.org/10.1016/j.gsf.2021.101245

Rampino, M. R., Haggety, B. M., & Pagano, T. C. (2006). A unified theory of impact crises and mass extinctions: Quantitative tests. *Annals of the New York Academy of Science*, *822*(1), 403–443. https://doi.org/10.1111/j.1749-6632.1997.tb48358.x

Rampino, M. R., & Prokoph, A. (2020). Are impact craters and extinction episodes periodic? Implications for planetary science and astrobiology. *Astrobiology*, *20*(9), 1097–1108. https://doi.org/10.1089/ast.2019.2043

Rampino, M. R., & Stothers, R. B. (1984a). Geological rhythms and cometary impacts. *Science*, *226*(4681), 1427–1431. https://doi.org/10.1126/science.226.4681.1427

Rampino, M. R., & Stothers, R. B. (1984b). Terrestrial mass extinctions, cometary impacts and the Sun's motion perpendicular to the galactic plane. *Nature*, *308*(5961), 709–712. https://doi.org/10.1038/308709a0

Raup, D. M. (1985). Magnetic reversals and mass extinctions. *Nature*, *314*(6009), 341–343. https://doi.org/10.1038/314341a0

Raup, D. M. (1991). A kill curve for Phanerozoic marine species. *Paleobiology*, *17*(1), 37–48. https://doi.org/10.1017/S0094837300010332

Raup, D. M., & Sepkoski, J. J., Jr. (1984). Periodicity and extinctions in the geological past. *Proceedings of the National Academy of Sciences USA*, *81*(3), 801–805. https://doi.org/10.1073/pnas.81.3.801

Renne, P. R., Deino, A. L., Hilgen, F. J., Kuiper, K. F., Mark, D. F., Mitchell, W. S., III, et al. (2013). Time scales of critical events around the Cretaceous-Paleogene Boundary. *Science*, *339*(6120), 684–687. https://doi.org/10.1126/science.1230492

Renne, P. R., Sprain, C. J., Richards, M. A., Self, S., Vanderkluysen, L., & Pande, K. (2015). State shift in Deccan volcanism at the Cretaceous-Paleogene boundary, possibly induced by impact. *Science*, *350*(6256), 76–78. https://doi.org/10.1126/science.aac7549

Rich, J. E., Johnson, G. L., Jones, J. E., & Campsie, J. (1986). A significant correlation between fluctuations in seafloor spreading rates and evolutionary pulsations. *Paleoceanography*, *1*, 85–95. https://doi.org/10.1029/PA001i001p00085

Richards, M. A., Alvarez, W., Self, S., Karlstrom, L., Renne, P. R., Manga, M., et al. (2015). Triggering of the largest Deccan eruptions by the Chicxulub impact. *Geological Society of America Bulletin*, *127*(11–12), 1507–1520. https://doi.org/10.1130/B31167.1

Robock, A., Oman, L., & Stenchikov, G. L. (2007). Nuclear winter revisited with modern climate model and current nuclear arsenals: Still catastrophic consequences. *Journal of Geophysical Research*, *112*(D13), D13107. https://doi.org/10.1029/2006JD008235

Rohde, R., & Muller, R. (2005). Cycles in fossil diversity. *Nature*, *434*(7030), 208–210. https://doi.org/10.1038/nature03339

Royer, D. L. (2014). Atmospheric CO_2 and O_2 during the Phanerozoic: Tools, patterns and impacts. In H. Holland & K. Turekian (Eds.), *Treatise on geochemistry* (2nd ed., pp. 251–267). Elselvier. ISBN 9780080983004.

Ruan, D., Chen, G., & Kerre, E. (2005). In G. Wets (Ed.), *Intelligent data mining: Techniques and applications, Studies in computational intelligence* (Vol. 5, p. 318). Springer. ISBN 978-3-540-26256-5.

Rudwick, M. (1997). *J. S. Georges Cuvier, Fossil bones, and geological catastrophes*. University of Chicago Press. ISBN 0-226-73106-5.

Sandberg, C. A., Morrow, J. R., & Ziegler, W. (2002). Late Devonian sea-level changes, catastrophic events, and mass extinctions. In *Geological Society of America Special Paper* (Vol. 356, pp. 473–487). https://doi.org/10.1130/0-8137-2356-6.473

Sanei, H., Grasby, S. E., & Beauchamp, B. (2012). Latest Permian mercury anomalies. *Geology*, *40*(1), 63–66. https://doi.org/10.1130/G32596.1

Santos, F. D., Ferreira, P. L., & Pedersen, J. S. T. (2022). The climate change challenge: A review of the barriers and solutions to deliver a Paris solution. *Climate*, *10*(5), 75. https://doi.org/10.3390/cli10050075

Scherer, L., Gürdal, İ., & van Bodegom, P. M. (2022). Characterization factors for ocean acidification impacts on marine biodiversity. *Journal of Industrial Ecology*, *2022*, 1–11. https://doi.org/10.1111/jiec.13274

Scherer, L., Svenning, J.-C., Huang, J., Seymour, C. L., Sandel, B., Mueller, N., et al. (2000). Global priorities of environmental issues to combat food insecurity and biodiversity loss. *Science of the Total Environment*, *730*, 139096. https://doi.org/10.1016/j.scitotenv.2020.139096

Schindewolf, O. H. (1954). Uber die möglichen Ursachen der grossen erdgeschichtlichen Faunenschnitte. *Neues Jahrbuch für Geologie und Palaontologie*, *1954/10*, 457–465.

Schindewolf, O. H. (1963). Neokatastrophismus? *Zeitschrift der Deutschen Geologischen Gesellschaft*, *114*(2), 430–445. https://doi.org/10.1127/zdgg/114/1963/430

Schlüter, L., Kai, T., Lohbeck, K. T., Gröger, J. P., Riebesell, U., & Reusch, T. B. H. (2016). Long-term dynamics of adaptive evolution in a globally important phytoplankton species to ocean acidification. *Science Advances*, *2*(7), e1501660. https://doi.org/10.1126/sciadv.1501660

Schmieder, M., & King, D. A. (2020). Earth's impact events through geologic time: A list of recommended ages for terrestrial impact structures and deposits. *Astrobiology*, *20*(1), 91–141. https://doi.org/10.1089/ast.2019.2085

Schobben, M., van de Schootbrugge, B., & Wignall, P. B. (2019). Interpreting the carbon isotope record of mass extinctions. *Elements*, *15*(5), 331–337. https://doi.org/10.2138/gselements.15.5.331

Schulte, P. (2010). The Chicxulub asteroid impact and mass extinction at the Cretaceous-Paleogene boundary. *Science*, *327*(5970), 1214–1218. https://doi.org/10.1126/science.1177265

Sepkoski, D. (2020). *Catastrophic thinking: Extinction and the value of diversity from Darwin to the Anthropocene*. University of Chicago Press. ISBN 978-0-226-34861-2.

Sepkoski, J. J. (1986). Phanerozoic overview of mass extinction. In D. M. Raup, & D. Jablonski (Eds.), *Patterns and processes in the history of life* (pp. 277–295). Springer-Verlag. https://doi.org/10.1007/978-3-642-79634-0_4

Sepkoski, J. J. (2002). A compendium of fossil marine animal genera. *Bulletins of American Paleontology*, *363*, 1–560.

Shen, J., Feng, Q., Algeo, T. J., Li, C., Planavsky, N. J., Zhou, L., & Zhang, M. (2016). Two pulses of oceanic environmental disturbance during the Permian-Triassic boundary crisis. *Earth and Planetary Science Letters*, *443*, 139–152. https://doi.org/10.1016/j.epsl.2016.03.030

Sheridan, R. E. (1987a). Pulsation tectonics as the control of continental breakup. *Tectonophysics*, *143*(1–3), 59–73. https://doi.org/10.1016/0040-1951(87)90078-3

Sheridan, R. E. (1987b). Pulsation tectonics as the control of long-term stratigraphic cycles. *Paleoceanography*, *2*, 97–118. https://doi.org/10.1029/PA002i002p00097

Sheridan, R. E. (1997). Pulsation tectonics as a control on the dispersal and assembly of supercontinents. *Journal of Geodynamics*, *23*(3–4), 173–196. https://doi.org/10.1016/s0264-3707(96)00047-6

Shi, D., Xu, Y., Hopkinson, B. M., & Morel, F. M. M. (2010). Effect of ocean acidification on iron availability to marine phytoplankton. *Science*, *327*(5966), 676–679. https://doi.org/10.1126/science.1183517

Sial, A. N., Chen, J., Lacerda, L. D., Peralta, S., Gaucher, C., Frei, R., et al. (2014). High-resolution Hg chemostratigraphy: A contribution to the distinction of chemical fingerprints of the Deccan volcanism and Cretaceous-Paleogene Boundary impact event. *Palaeogeography, Palaeoclimatology, Palaeoecology*, *414*, 98–115. https://doi.org/10.1016/j.palaeo.2014.08.013

Sial, A. N., Lacerda, L. D., Ferreira, V. P., Frei, R., Marquillas, R. A., Barbosa, J. A., et al. (2013). Mercury as a proxy for volcanic activity during extreme environmental turnover: The Cretaceous-Paleogene transition. *Palaeogeography, Palaeoclimatology, Palaeoecology*, *387*, 153–164. https://doi.org/10.1016/j.palaeo.2013.07.019

Sigman, D. M., & Boyle, E. A. (2000). Glacial/interglacial variations in atmospheric carbon dioxide. *Nature*, *407*(6806), 859–869. https://doi.org/10.1038/35038000

Smyrnova, L., Katunina, E., Rjabinin, A., & Anninskaja, I. (2017). The impact of atmospheric precipitation (rainfalls) on the sea-surface microlayer in the Sevastopol coastal waters (Crimea, the Black Sea). *Ecologica Montenegrina*, *14*, 30–38. https://doi.org/10.37828/em.2017.14.4

Song, H., Kemp, D. B., Tian, L., Chu, D., Song, H., & Dai, X. (2021). Thresholds of temperature change for mass extinctions. *Nature Communications*, *12*(1), 4694. https://doi.org/10.1038/s41467-021-25019-2

Stanley, S. M. (2016). Estimates of the magnitudes of major marine mass extinctions in Earth history. *Proceedings of the National Academy of Sciences USA*, *113*(42), E6325–E6334. https://doi.org/10.1073/pnas.1613094113

Sun, D., Wignal, P. B., Joacimski, M. M., Bond, D. P. G., Grasby, S. E., Lai, X. L., et al. (2016). Climate warming, euxinia and carbon isotope perturbations during the Carnian (Triassic) crisis in South China. *Earth and Planetary Science Letters*, *444*, 88–100. https://doi.org/10.1016/j.epsl.2016.03.037

Sun, Y., Joachimski, M. M., Wignall, P. B., Yan, C., Chen, Y., Jiang, H., et al. (2012). Lethally hot temperatures during the early Triassic greenhouse. *Science*, *338*(6105), 366–370. https://doi.org/10.1126/science.1224126

Tapan, H. (1968). Primary production, isotopes, extinctions and the atmosphere. *Paleoecology*, *4*(3), 187–210. https://doi.org/10.1016/0031-0182(68)90047-3

Tennant, J., Mannion, P., & Upchurch, P. (2016). Sea level regulated tetrapod diversity dynamics through the Jurassic/Cretaceous interval. *Nature Communications*, *7*(1), 12737. https://doi.org/10.1038/ncomms12737

Tennant, J. P., Mannion, P. D., & Upchurch, P. (2016). Environmental drivers of crocodyliform extinction across the Jurassic/Cretaceous transition. *Proceedings of the Royal Society B*, *283*(1826), 20152840. https://doi.org/10.1098/rspb.2015.2840

Thibodeau, A. M., Ritterbush, K., Yager, J. A., West, A. J., Ibarra, Y., Bottjer, D. J., et al. (2016). Mercury anomalies and the timing of biotic recovery following the end-Triassic mass extinction. *Nature Communications*, *7*(1), 11147. https://doi.org/10.1038/ncomms11147

Tiwari, R. K., & Rao, K. N. N. (1998). Correlated variations and periodicity of global CO_2, biological mass extinctions and extra-terrestrial bolide impacts over the past 250 million years and possible geodynamical implications. *Geofizika*, *215*, 103–117. Retrieved from https://hrcak.srce.hr/17773

Twitchett, R. J. (2006). The palaeoclimatology, palaeoecology and palaeoenvironmental analysis of mass extinction events. *Palaeogeography, Palaeoclimatology, Palaeoecology*, *232*(2–4), 190–213. https://doi.org/10.1016/j.palaeo.2005.05.019

University of Chicago. (2022). Retrieved from http://climatemodels.uchicago.edu/modtran

Urey, H. C. (1973). Cometary collisions and geological periods. *Nature*, *242*(5392), 32–33. https://doi.org/10.1038/242032a0

Van Avendonk, H. J. A., Davis, J. K., Harding, J. L., & Lawver, L. A. (2016). Decrease in oceanic crustal thickness since the breakup of Pangaea. *Nature Geosciences*, *10*(1), 58–61. https://doi.org/10.1038/nge02849

Van Der Meer, D. G., Zeebe, R. E., van Hinsbergen, D. J. J., Sluijs, A., Spakman, W., & Torsvik, T. H. (2014). Plate tectonic controls on atmospheric CO_2 levels since the Triassic. *Proceedings of the National Academy of Sciences USA*, *111*(12), 4380–4385. https://doi.org/10.1073/pnas.1315657111

VanderZwaag, D. L., Oral, N., & Stephens, T. (Eds.). (2021). *Research handbook on ocean acidification law and policy*. Edward Elgar Publishing. ISBN 978 1 78990 014 9 (eBook). https://doi.org/10.4337/9781789900149

Veizer, J., Ala, D., Azmy, K., Bruckschen, P., Buhl, D., Bruhn, F., et al. (1999). $^{87}Sr/^{86}Sr$, $\delta^{13}C$ and $\delta^{18}O$ evolution of Phanerozoic seawater. *Chemical Geology*, *161*(1–3), 59–88. https://doi.org/10.1016/S0009-2541(99)00081-9

Veizer, J., & Prokoph, A. (2015). Temperature and oxygen isotopic composition of Phanerozoic oceans. *Earth-Science Reviews*, *146*, 92–104. https://doi.org/10.1016/j.earscirev.2015.03.008

Vellekoop, J., Sluijs, A., Smit, J., Schouten, S., Weijers, J. W. H., Damsté, J. S. S., & Brinkhuis, H. (2014). Rapid short-term cooling following the Chicxulub impact at the Cretaceous-Paleogene boundary. *Proceedings of the National Academy of Sciences USA*, *111*(21), 7537–7541. https://doi.org/10.1073/pnas.1319253111

Vernon, J. E. N. (2008). Mass extinctions and ocean acidification: Biological constraints on geological dilemmas. *Coral Reefs*, *27*(3), 459–472. https://doi.org/10.1007/s00338-008-0381-8

Vinós, J. (2022). Greenhouse gases and climate change. In J. Vinós (Ed.), *Climate of the past, present and future. A scientific debate* (2nd ed.). Critical Science Press. ISBN 978-84-125867-0-1.

Vogt, P. R. (1972). Evidence for global synchronism in mantle plume convection and possible significance for geology. *Nature*, *240*(5380), 338–342. https://doi.org/10.1038/240338a0

Walliser, O. (Ed.) (1996). *Global events and event stratigraphy in the phanerozoic* (p. 333). Springer-Verlag. ISBN 978-3-642-79634-0.

Wang, L.-N., Wignall, P. B., Wang, Y.-B., Jiang, H.-S., Sun, Y.-D., Li, G.-S., et al. (2016). Depositional conditions and revised age of the Permo-Triassic microbialites at Gaohua section, Cili County (Hunan Province, South China). *Palaeogeography, Palaeoclimatology, Palaeoecology*, *443*, 156–166. https://doi.org/10.1016/j.palaeo.2015.11.032

Ward, P. D., Montgomery, D. R., & Smith, R. (2000). Altered river morphology in South Africa related to the Permian-Triassic extinction. *Science*, *289*(5485), 1740–1743. https://doi.org/10.1126/science.289.5485.1740

Weinbauer, M. G., Mari, X., & Gattuso, J.-P. (2012). Effects of ocean acidification on the diversity and activity of heterotrophic marine microorganisms. In J.-P. Gattuso & L. Hansson (Eds.), *Ocean acidification* (pp. 83–98). Oxford University Press. ISBN 978-0-19-959108-4.

Wignall, P. B. (2015). *The worst of times: How life on Earth survived eighty million years of extinction*. Princeton University Press. ISBN 978-0-691-14209-8.

Wignall, P. B., & Hallam, A. (1992). Anoxia as a cause of the Permian/Triassic extinction: Facies evidence from northern Italy and the western United States. *Palaeogeography, Palaeoclimatology, Palaeoecology*, *93*(1–2), 21–46. https://doi.org/10.1016/0031-0182(92)90182-5

Wignall, P. B., & Twitchett, R. J. (1996). Oceanic anoxia and the End Permian mass extinction. *Science*, *272*(5265), 1155–1158. https://doi.org/10.1126/science.272.5265.1155

Wilf, P., Johnson, K. R., & Huber, B. T. (2003). Correlated terrestrial and marine evidence for global climate changes before mass extinction at the Cretaceous-Paleogene boundary. *Proceedings of the National Academy of Sciences USA*, *100*(2), 599–604. https://doi.org/10.1073/pnas.0234701100

Wolfram, U., Peña Fernández, M., McPhee, S., Smith, E., Beck, R. J., Shephard, J. D., et al. (2022). Multiscale mechanical consequences of ocean acidification for cold-water corals. *Scientific Reports*, *12*(1), 8052. https://doi.org/10.1038/s41598-022-11266-w

Wu, Y., Chu, D., Tong, J., Song, H., Dal Corso, J., Wignall, P. B., et al. (2021). Six-fold increase of atmospheric pCO_2 during the Permian–Triassic mass extinction. *Nature Communications*, *12*(1), 2137. https://doi.org/10.1038/s41467-021-22298-7

Wurl, O., Ekau, W., Landing, W. M., & Zappa, C. J. (2017). Sea surface microlayer in a changing ocean – A perspective. *Elementa: Science of the Anthropocene*, *5*, 31. https://doi.org/10.1525/elementa.228

Zeebe, R. E., & Zachos, J. C. (2013). Long-term legacy of massive carbon input to the Earth system: Anthropocene versus Eocene. *Philosophical Transactions of the Royal Society A*, *371*(2001), 20120006. https://doi.org/10.1098/rsta.2006.1794

Zhu, Z., Liu, Y., Kuang, H., Benton, M. J., Newell, A. J., Xu, H., et al. (2019). Altered fluvial patterns in North China indicate rapid climate change linked to the Permian-Triassic mass extinction. *Nature, Science Reports*, *9*(1), 16818. https://doi.org/10.1038/s41598-019-53321-z

Zunino, S., Libralato, S., Canu, D. M., Prato, G., & Solidoro, C. (2021). Impact of ocean acidification on ecosystem functioning and services in habitat-forming species and marine ecosystems. *Ecosystems*, *24*(7), 1561–1575. https://doi.org/10.1007/s10021-021-00601-3

Erratum

In the originally published article, in the third sentence of the fifth paragraph of Section 3.3, the word "here" was repeated, and the sentence read: "This pattern, identified previously for the K-Pg extinction (L. Alvarez et al., 1984) is here confirmed here for all past mass extinctions, providing new constraints on the nature and causes of mass extinctions (Section 4)." The sentence has been corrected to read as follows: "This pattern, identified previously for the K-Pg extinction (L. Alvarez et al., 1984) is confirmed here for all past mass extinctions, providing new constraints on the nature and causes of mass extinctions (Section 4)." This may be considered the authoritative version of record.